T.R.

GEBZE TECHNICAL UNIVERSITY

GRADUATE SCHOOL OF NATURAL AND APPLIED SCIENCES

PREPARATION AND CHARACTERIZATION OF MICROSTRUCTURALLY ENGINEERED TEXTURED 0.9PMN-0.1PT PIEZOELECTRIC CERAMICS

YUSUF KILIÇ

A THESIS SUBMITTED FOR THE DEGREE OF

MASTER OF SCIENCE

DEPARTMENT OF MATERIALS SCIENCE AND ENGINEERING

GEBZE

2019

T.R.

GEBZE TECHNICAL UNIVERSITY

GRADUATE SCHOOL OF NATURAL AND APPLIED SCIENCES

PREPARATION AND CHARACTERIZATION OF MICROSTRUCTURALLY ENGINEERED TEXTURED 0.9PMN-0.1PT PIEZOELECTRIC CERAMICS

YUSUF KILIÇ

A THESIS SUBMITTED FOR THE DEGREE OF

MASTER OF SCIENCE

DEPARTMENT OF MATERIALS SCIENCE AND ENGINEERING

THESIS SUPERVISOR

PROF. DR. EBRU MENŞUR ALKOY

GEBZE

2019

T.C.
GEBZE TEKNİK ÜNİVERSİTESİ
FEN BİLİMLERİ ENSTİTÜSÜ

0.9PMN-0.1PT DOKULU PİEZOELEKTRİK SERAMİKLERİNİN ÜRETİMİ VE KARAKTERİZASYONU

YUSUF KILIÇ
YÜKSEK LİSANS TEZİ
MALZEME BİLİMİ VE MÜHENDİSLİĞİ ANABİLİM DALI

DANIŞMANI
PROF. DR. EBRU MENŞUR ALKOY

GEBZE
2019

GEBZE TEKNİK ÜNİVERSİTESİ	**YÜKSEK LİSANS JÜRİ ONAY FORMU**

GTÜ Fen Bilimleri Enstitüsü Yönetim Kurulu'nun 30/05/2019 tarih ve 2019/25 sayılı kararıyla oluşturulan 10/06/2019 tarihinde tez savunma sınavı yapılan Yusuf KILIÇ'ın tez çalışması Malzeme Bilimi ve Mühendisliği Anabilim Dalında YÜKSEK LİSANS tezi olarak kabul edilmiştir.

JÜRİ

ÜYE (TEZ DANIŞMANI) : PROF. DR. EBRU MENŞUR-ALKOY

ÜYE : PROF. DR. HÜSEYİN YILMAZ

ÜYE : DR. ÖĞR. ÜYESİ AYŞE BERKSOY-YAVUZ

ONAY

Gebze Teknik Üniversitesi Fen Bilimleri Enstitüsü Yönetim Kurulu'nun …/…/… tarih ve …/… sayılı kararı.

İMZA / MÜHÜR

Prof. Dr. Arif Çağdaş AYDINOĞLU
Gebze Teknik Üniversitesi
Fen Bilimleri Enstitüsü Müdürü

SUMMARY

Lead-based piezoelectric materials are known with their high electrical and electromechanical properties for potential applications. Among various lead-based piezoelectric materials, $(1-x)Pb(Mg_{1/2}Nb_{2/3})O_3–(x)PbTiO_3$ ceramics (abbreviated as PMN-PT) are promising materials for transducers, medical ultrasound, ultrasonic motors and actuators. In this study, 0.9PMN-0.1PT was chosen due to relaxor ferroelectric response of this composition. Piezoelectric ceramic powders were synthesized by solid-state reaction route. The final PMN-PT particle size of the powders was measured as 0.18 μm. The samples of 0.9PMN-0.1PT were prepared with two methods as dry-pressing and tape-casting. Moreover, barium titanate ($BaTiO_3$) template particles were synthesized by molten salt synthesis method and were used to texture the 0.9PMN-0.1PT with ratio of 5%-vol. A combination of tape-casting and template grain growth was used to obtain textured PMN-PT samples. All samples were sintered at 1150^oC for various durations. Microstructural and compositional analyses have been carried out using scanning electron microscope (SEM) and X-ray diffraction (XRD). Dielectric and ferroelectric properties have been investigated. Pure perovskite structure was obtained in all sintered samples. Temperature-depended measurement of dielectric constant was performed. Electric field-induced strain was measured as ~0.14% at 30 kV/cm. The Curie temperatures were measured at 1 kHz, 10 kHz and 100 kHz as 41°C, 43°C and 45°C for dry-pressing samples and 39°C, 41°C and 43°C for textured samples, respectively, indicating the relaxor nature of the ceramics. Remnant polarization (P_r) of non-textured sample was measured as ~$2P_r$ =12.7 μC/cm^2 at 30 kV/cm and was also measured as 6.4 μC/cm^2 at 30 kV/cm for the textured sample.

Key Words: Lead-based, PMN-PT, Textured, Template Particle.

ÖZET

Kurşun esaslı piezoelektrik malzemelerin yüksek elektriksel ve elektromekanik özellikler gösterdiği bilinmektedir. Çeşitli kurşun esaslı piezoelektrik malzemeler arasında, perovskite yapıya sahip (1-x)Pb($Mg_{1/2}Nb_{2/3}$)O_3–(x)$PbTiO_3$ (PMN-PT) seramikleri transdüserler, ultrasonik motorlar, aktüatörler ve tıbbi ultrason gibi birçok uygulama için potansiyel malzemelerdir. Bu çalışmada, relaksör ferroelektrik özelliği nedeniyle 0.9PMN-0.1PT kompozisyonu seçilmiştir. Piezoelektrik seramikler katı hal reaksiyon yolu ile sentezlenmiştir. Nihai PMN-PT partikül boyutu 0.18 μm'dir ve bu partikül boyutu yoğun piezoelektrik seramik elde etmek için yeterlidir. 0.9PMN-0.1PT numuneleri kuru presleme ve şerit döküm olmak üzere iki yöntemle hazırlanmıştır. $BaTiO_3$ şablon parçacıkları ergimiş tuz sentezi yöntemiyle sentezlenmiş ve dokulandırmak için %5-hacim oranında kullanılmıştır. Dokulu PMN-PT numuneleri elde etmek için şerit döküm ve şablonlu tane büyümesi kombinasyonu kullanılmıştır. Numuneler 1150°C'de farklı sürelerde sinterlenmiştir. Taramalı elektron mikroskobu (SEM) ve X-ışını difraksiyonu (XRD) kullanılarak mikroyapısal analizler ve faz analizleri yapılmıştır. Dielektrik ve ferroelektrik özellikler incelenmiştir. Tüm sinterlenmiş numunelerde saf perovskit yapısı elde edilmiştir. Dielektrik sabitinin sıcaklığa bağlı ölçümü yapılmıştır. Elektrik alan kaynaklı gerinme 30 kV/cm'de ~% 0.14 olarak ölçülmüştür. Curie sıcaklıkları, kuru presleme numuneleri için sırasıyla 1 kHz, 10 kHz ve 100 kHz'de 41°C, 43°C ve 45°C ve dokulu numunelerde sırasıyla 39°C, 41°C ve 43°C olarak ölçülmüştür. Dokulu olmayan numunenin kalıntı polarizasyonu (P_r) 30 kV/cm'de ~$2P_r$ =12.7 μC/cm^2 olarak ölçülmüş ve dokulu numune için kalıntı polarizasyon 30 kV/cm'de 6.4 μC/cm^2 olarak ölçülmüştür.

Anahtar Kelimeler: Kurşun esaslı, PMN-PT, Dokulu, Şablon Parçaçık.

ACKNOWLEDGEMENTS

First of all, my biggest gratefulness is to my advisor, mentor and pathfinder Prof. Ebru MENŞUR-ALKOY for giving her full support to me in writing this thesis and doing all our scientific researches. This support and trust encouraged me to going further and being better every time. I would like to thank to Prof. Sedat ALKOY for answering my endless questions, giving his advises and support for this study.

I would like to thank Assoc. Prof. Ayşe BERKSOY YAVUZ, Res. Asst. Namık Kemal GÖZÜAÇIK and Ömer ÇAKMAK for all of their support and fruitful discussions. I would like to thank Adem ŞEN and Ahmet NAZIM for their help on this study. I would like to thank all "Piezo Research Group" members for their support.

Lastly, the most special gratitude to my mother Kadriye KILIÇ, my father Bahri KILIÇ, my sister Esin BAL, my brother Alper Can KILIÇ, my niece Ezgi Hira BAL and to all my dear friends for their endless support.

I also wish to acknowledge the financial support of AFOSR Project Award #FA9550-18-1-0450.

TABLE of CONTENTS

LIST of ABBREVIATIONS and ACRONYMS

Abbreviations and Acronyms		**Explanations**
Å	:	Angstrom
cm	:	Centimeter
E_C	:	Coercive Field
C	:	Coulomb
T_C	:	Curie Temperature
^oC	:	Degree Celsius
K	:	Dielectric Constant
tanδ	:	Dielectric Dissipation Factor
E	:	Electric Field
Hz	:	Hertz
h	:	Hour
kHz	:	Kilohertz
kV	:	Kilovolt
kV/cm	:	Kilovolt per centimeter
P_{max}	:	Maximum polarization
MPa	:	Megapascal
m	:	Meter
m^2	:	Meter square
μm	:	Micrometer
$\mu C/cm^2$	:	Microcoulomb per centimeter square
min	:	Minute
MPB	:	Morphotropic Phase Boundary
%	:	Percentage
P_r	:	Remnant Polarization
P_s	:	Spontaneous Polarization
S	:	Strain
V	:	Voltage
$BaTiO_3$	:	Barium Titanate
PMN	:	Lead Magnesium Niobate

PT	:	Lead Titanate
PZ	:	Lead Zirconate
PZT	:	Lead Zirconate Titanate
SEM	:	Scanning Electron Microscope
~	:	Tilde
wt	:	Weight
XRD	:	X-ray Diffraction

LIST of FIGURES

LIST of TABLES

1. INTRODUCTION

Lead-based ferroelectric ceramics are known to exhibit high electrical and electromechanical properties. $Pb(Mg_{1/2}Nb_{2/3})O_3$–$PbTiO_3$ (PMN-PT) ceramics with perovskite structure are potential materials for many applications such as transducers, medical ultrasound, ultrasonic motors and actuators due to their high piezoelectric, dielectric and electromechanical coupling coefficients.

Lead magnesium niobate (PMN) is the most common ferroelectric with a maximum dielectric constant at about -10°C. Another characteristic of the relaxor is the dıffuse phase transition. That is, the exact temperature at which the phase transition occurs is not fully visible and therefore the phase transition is independent of the temperature. But the phase transition is dependent from frequency.The high permeability of the relaxor and the independence from the temperature (Dıffuse phase transition) is a great advantage, while the other characteristic dielectric relaxation behavior adds a negative characteristic [1].

PMN-based relaxor ceramics have a wide range of applications as high strain (0.1%) electrositritive actuators and high dielectric constant capacitors [2]. $Pb(Mg_{1/3}Nb_{2/3})O_3$ (PMN) is a good voltage stability, superior electrostrictive effect, low sintering temperature (<1000°C) and a relaxor ferroelectric material having a high dielectric constant of 15000 at a frequency of 1 kHz at the Curie temperature [3]. However, PMN has a Curie temperature of -15°C and is limited for many applications [4]. The addition of normal ferroelectric $PbTiO_3$ (PT), whose curie temperature is 490°C, increases the T_c of the PMN to a higher temperature [5]. The solid solution formed between the PMN and the PT not only increases the Tc of the PMN, but also changes its dielectric properties, electromechanical properties and phase transformations.

Lead magnesium niobate (PMN)-lead titanate (PT) [$Pb(Mg_{1/3}Nb_{2/3})O_3$-$PbTiO_3$] piezoelectric ceramics of 0.9PMN-0.1PT were specifically chosen for this study because of relaxor ferroelectric properties of this composition. Piezoelectric ceramics were synthesized by modified solid-state reaction route and tape casting and their electrical measurements and structural examinations were also performed for PMN-PT samples. The dielectric, ferroelectric and piezoelectric properties of the PMN-PT system were studied in detail.

1.1. Aim of Thesis

$(1-x)Pb(Mg_{1/2}Nb_{2/3})O_3–(x)PbTiO_3$ (PMN-PT) solid solution, which has perovskite type structure, demonstrates very good electrostrictive (relaxor) or piezoelectric (ferroelectric) properties depending on their content. These features are very useful for many applications. In thesis study, lead magnesium niobate (PMN)-lead titanate (PT) $[Pb(Mg_{1/3}Nb_{2/3})O_3\text{-}PbTiO_3]$ piezoelectric ceramics as 0.9PMN-0.1PT was specifically chosen because of relaxor ferroelectric properties of this composition with low phase transformation temperature. Ceramic samples were fabricated by dry-pressing and tape-casting method. However, textured ceramics with 5% barium titanate (BT) were fabricated by tape-casting method. Structural and electrical properties of these samples were performed in detail.

2. LITERATURE REVIEW

2.1. Electroceramics

Electroceramics, a subgroup of advanced ceramics, have been used in many electronic applications since the middle of the 20th century with the presence of materials with high dielectric constant (such as barium titanate). Electroceramics have a large market share in ceramic ındustry since they have high added value despite the low percentage of usage of other advanced ceramics in the world. Electroceramic materials are used in capacitors, heaters, electreds, gas detectors, varistors, thermistors, and solid oxide fuel cells thanks to their dielectric, electromechanical and electrooptical properties. However, piezoelectric ceramics are generally used in electromechanical applications for underwater imaging, listening, communication (sonar, hydrophone), automatic firing systems, medical imaging (ultrasound) [6].

2.2. Piezoelectric Properties

The word “piezo” is of Greek origin and corresponds to either jamming or mechanical force. The piezoelectricity was discovered by the Jacques-Pierre Curie brothers in 1880, when materials such as quartz, tourmaline and sphalerite, which constitute electrical potential in response to a applied mechanical force, were found [2].

In order to observed a piezoelectric effect, material has to be a non centro-symmetric in the unit cell structure. In this case, all ferroelectric materials have piezoelectric properties due to their polar structures in crystal lattice [7]. According to the Neumann principle, the symmetry of any physical property of a crystal must include the symmetry of this crystalline point group [8].

As shown in Figure 2.1, the crystals that were divided into 32 point groups formed from seven crystal systems, and 21 of these groups do not have a symmetry center. 10 of the remaining 20 point groups are polarized under mechanical force while the other half are self-polarizing. Below these 10 point groups with permanent polarization, there is a sub-group of materials that exhibit spontaneous and re-

orientable polarization. This sub-group exhibits all of its ferroelectric, piezoelectric and pyroelectric properties [2].

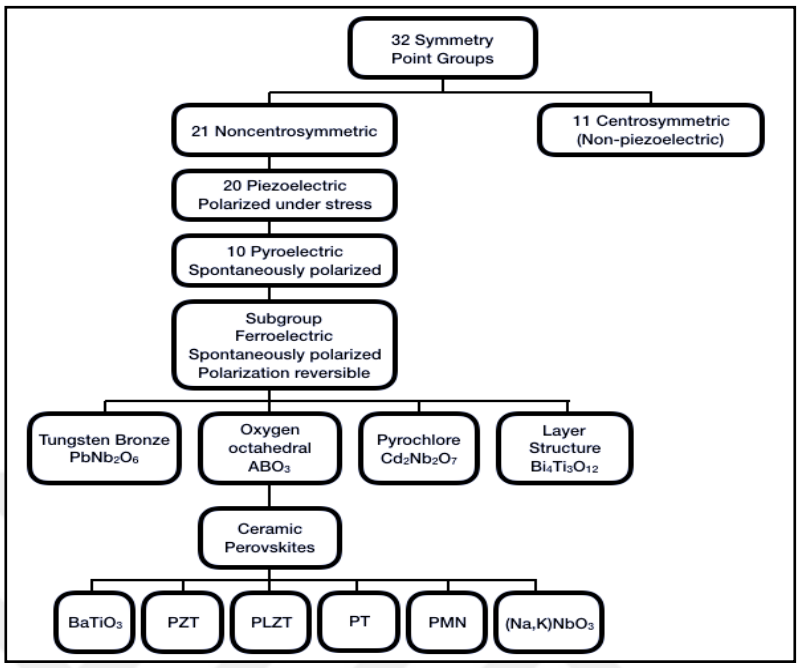

Figure 2.1: Interrelationship of piezoelectric and subgroups on the basis of symmetry.

Direct Piezoelectric Effect: A change in the dipole moments occurs due to the compression and tensile stress that occurs in the polarized material, and an electrical potential difference occurs with the accumulation of charge on the surface.

Indirect Piezoelectric Effect: The electrical field in the crystal size is thus cause a change in volume. These situations are shown in Figure 2.2 [2].

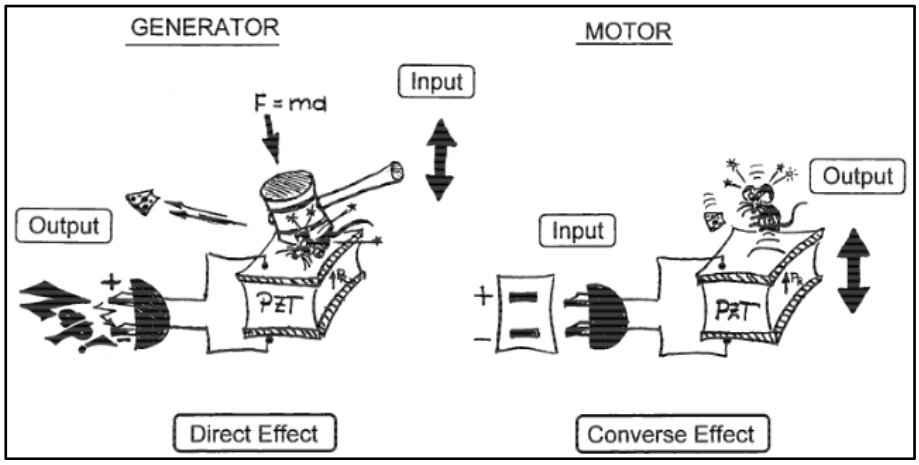

Figure 2.2: Direct and converse piezoelectric effect.

2.3. Ferroelectric Properties

Ferroelectricity is one of the most interesting features of dielectric solids. These can be single crystals, but also in the form of a highly crystalline (polycrystalline) solid. In normal dielectric materials, the polarization formed by an electric field applied externally is very small, the dielectric constant is generally less than 100, and the dielectric constant in the ferroelectric materials is up to 10000s. It can be defined by self-polarization which can be redirected by electric field effect. At the temperature of the curie (T_c) the material loses its ferroelectric property and exhibits normal dielectric behavior which is called as paraelectric state. Ferroelectric materials generally exhibit nonpolar behavior at temperatures below T_c and have a very high dielectric constant, especially in regions close to Curie temperature [9]. The electric field applied initially to an unpolarized disc has an effect sufficient to align the dipoles in the crystals, and the polarization increases linearly with the applied electric field. Since the electric field reaches a certain value, the orientation of the dipoles will start to stabilize and an increasing in polarization is observed. In a higher electric field, the polarization reaches the saturation point (P_{max}). Remnant polarization (P_r) is that the polarization is not zero when the electric field is not applied. The direction of polarization can be changed depending on the applied electric field [9]. The most prominent feature in ferroelectrics is the hysteresis loop between the polarization (P) and the applied electric field (E) which is shown in Figure 2.3 [which was taken from the sample produced in this study].

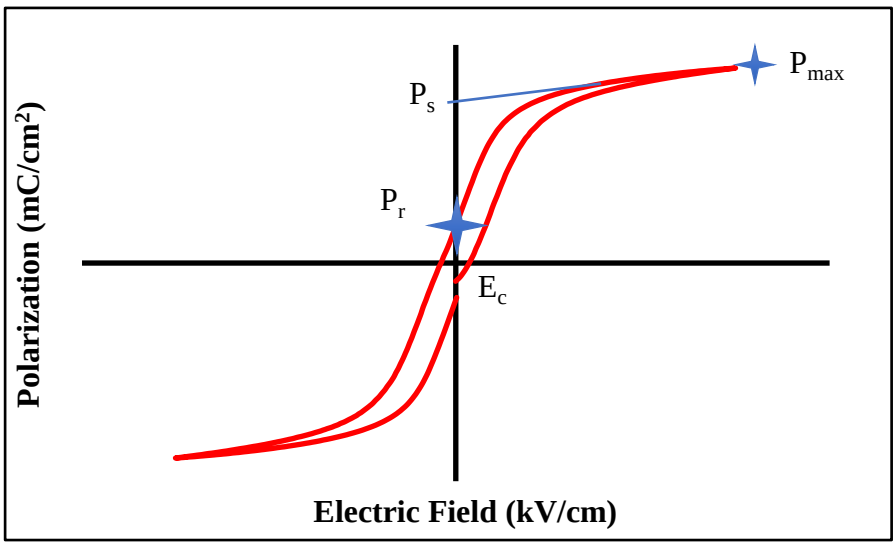

Figure 2.3: P-E hysteresis loop.

When the electric field is reduced to zero, the material has a clear remanent polarization (P_r). Then, if the electric field continues to be applied in the opposite direction, the polarization also reaches the saturation point in the opposite direction due to the resulting electric field, thus completing the hysteresis cycle. The electric field is called the coercive electric field (E_c) where the polarization is equal to zero [10].

A piezoelectric ceramic may be considered to consist of randomly oriented piezoelectric crystals. Net piezoelectric activity is zero due to this random orientation. Piezoelectricity cannot be observed until the direction of the dipoles are in the same state through the ceramic. Exceeding this situation is possible with special production methods such as extrusion and hot forging. In addition, the polarization process, which is a much easier method, is widely applied. As shown in Figure 2.4 [11], a silver electrode coated ceramics, which are parallel to each other, can be made piezoelectric in the direction of a pole selected by a polarization process in which they are exposed to a high electric field. The polarization is carried out under T_c and the application of an electric field of about one quarter of the hysteresis loop. If the material reaches permanent polarization, the polarization process is terminated. In addition, the presence of polarization and ferroelectricity has also made it possible to produce synthetic piezoelectrics [10].

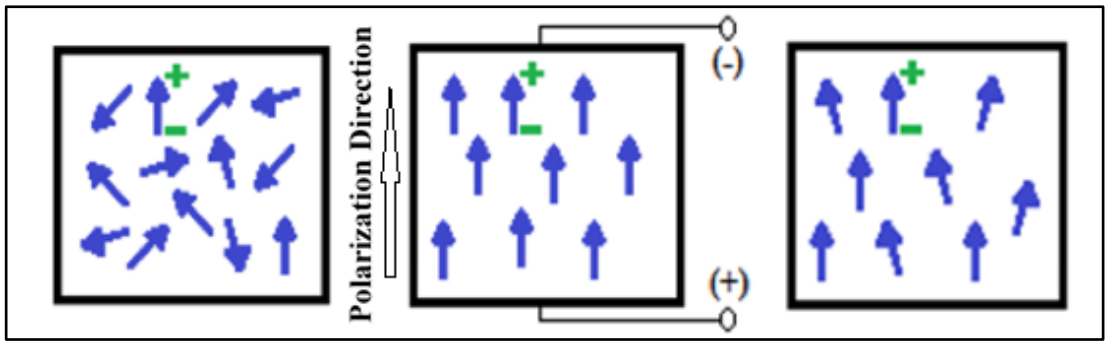

Figure 2.4: Polarization change of piezoceramic materials with electric field.

There are four types of ferroelectric ceramics given as sub-categories of general ferroelectric material groups. These are grouped according to the unit cell structures as follows [2];

- Perovskite structure with oxygen octahedra (ABO_3)
- Tungsten bronze structure

- Pyrochlorine structure
- Bismuth layer structure

Ferroelectric ceramics, which are one of the first materials, are the most used group with the highest market share and have ABO_3 perovskite structure. Barium titanate ($BaTiO_3$), lead zirconate-titanate (PZT), lead magnesium niobate-lead titanate (PMN-PT) and sodium-potassium niobate $(Na,K)NbO_3$ compositions are commercially produced ferroelectric materials in the world today. Another group, the tungsten bronze structure, was discovered in 1952 by Goodman as the lead niobate (PN) [12].

2.4. Perovskite Structure

Perovskite structure has the general formula of ABO_3. In general, A atoms are placed at corners of cubic structures, B atoms are located in spaces of oxygen octhohedral center and oxygen atoms are placed in surface centers of cubic structure, as shown in Figure 2.5., and as seen as $CaTiO_3$ minerals. The large Ca^{2+} cation in position A is surrounded by O^{2-} anions and the Ti^{4+} cation has 6 coordination number [13]. Large cations (such as Pb^{2+}, Ba^{2+}, Bi^{3+}, Na^{+}) with 12 corners, smaller cations (Ti^{4+}, Zr^{4+}, Nb^{5+}, Mg^{2+}) are octahedrally coordinated with oxygen [14]. The fact that most perovskite structures exhibit ferroelectric and piezoelectric properties and high dielectric constant make the perovskite structure important [6]. Many relaxors are ferroelectric, $Pb(B'B'')O_3$ compounds with a lead-based perovskite structure. B' and B'' consist of two different ionic loads. To ensure load neutrality, the valence average of these two B position cations should be +4 [15].

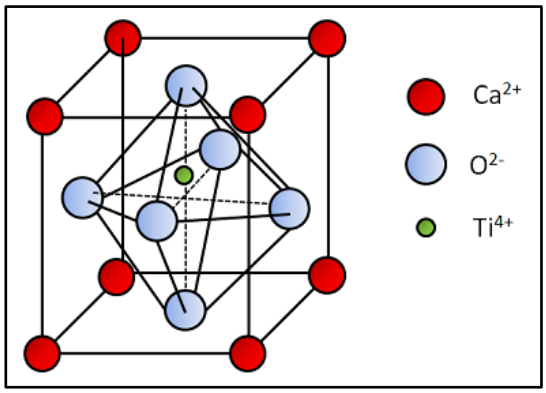

Figure 2.5: A perovskite unit cell.

2.5. Relaxor Ferroelectrics and PMN-PT Solid Solution

Relaxor ferroelectrics are lead-based complex perovskite structures. In general, $Pb(B'B'')O_3$ is the formula. Here, B' is composed of low-valence cations such as Mg^{2+}, Zn^{2+} or S^{3+}, B'' is composed of high-valence cations such as Nb^{5+} or Ta^{5+} [16].

The production of multi-layer ceramic capacitors has been reduced with the realization that the relievers have low sintering temperature and high permeability. On the other hand, it has been the driving force for actuators due to its high electrostrictive coefficients [17]. Three prominent features of the relaxors are; high permeability, diffuse phase transition (DPT) and dielectric relaxation [1].

Lead magnesium niobate (PMN) is the most common ferroelectric with a maximum dielectric constant at about -10°C. Another characteristic of the relaxor is the diffuse phase transition. That is, the exact temperature at which the phase transition occurs is not fully visible and therefore the phase transition is independent of the temperature. The high permeability of the relaxor and the independence from the temperature (diffuse phase transition) is a great advantage, while the other characteristic dielectric relaxation behavior is a disadvantage [1].

High permeability is mainly due to the fact that the two ions, which are located in position B, have different values and different dimensions. These two ions, one is big and the other is small, are irregularly located in the B position as shown in Figure 2.6. Large ions expand the neighboring lattice structure and facilitate movement in this cage where the small ion is placed. Therefore, when the electric field is applied to the material, the ions have a very large dielectric constant due to their comfortable displacement in large volumes [1].

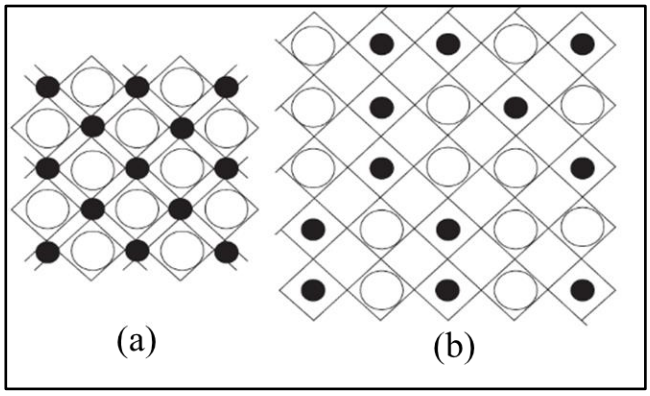

Figure 2.6: $A(B_{I1/2}B_{II1/2})O_3$ perovskite type crystal model, a) small movable hollow regular, b) large moving hollow irregular structure.

In addition to this irregular distribution in the crystal lattice, there are also some small regular regions. These regular regions (2-5 nm) normally show ferroelectric properties. In the structure of PMN, these regular and irregular regions coexist and each region behaves as if it has different Curie temperature. Therefore, a propagation is observed in the phase transition.

The relaxor behavior is that the permeability changes depending on the frequency. Normally, the perovskite structure has two potential equilibrium positions when it passes to the ferroelectric phase, and a single equilibrium position in the paraelectric phase. However, as a result of the irregular distribution of ions in the relaxors, more than one shallow potential minimum occurs in each latice. When the electric field is applied, the ion movement increases with the increase of the frequency, becomes untraceable and the dielectric constant starts to decrease [1].

As seen in Figure 2.10, the permeability in the relaxor, as a function of temperature with a distinct frequency separation, shows a wide peak distribution in contrast to normal ferroelectrics [18].

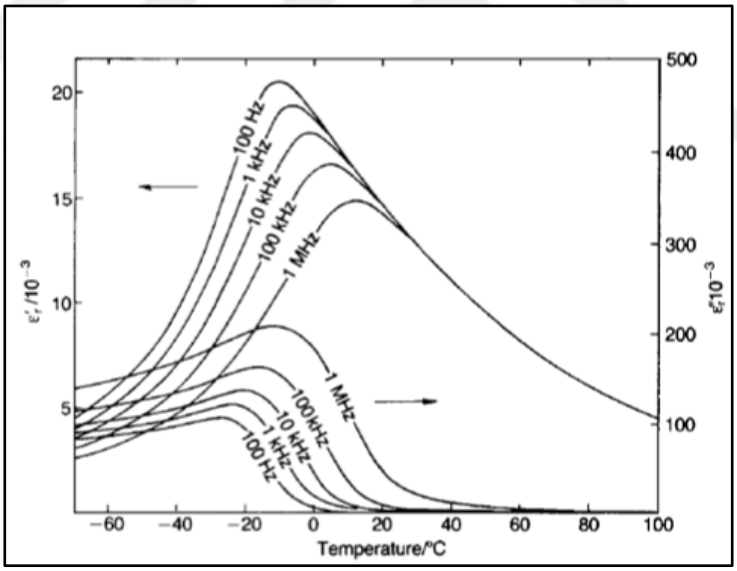

Figure 2.7: Dielectric constant and temperature graph of relaxor system.

PMN-based relaxor ceramics have a wide range of applications such as high strain (0.1%) electrostrictive actuators and high dielectric constant capacitors [2]. Pb $(Mg_{1/3}Nb_{2/3})O_3$ (PMN) has a good voltage stability, superior electrostrictive effect, low sintering temperature (< 1000°C) and a relaxor ferroelectric material having a high dielectric constant of 15000 at a frequency of 1 kHz at the Curie temperature [3]. However, PMN has a Curie temperature of -15°C and is limited for many

applications [4]. The addition of normal ferroelectric $PbTiO_3$ (PT), whose Curie temperature is 490°C, increases the T_c of the PMN to a higher temperature [5]. The solid solution formed between the PMN and the PT not only increases the T_c of the PMN, but also changes its dielectric properties, electromechanical properties and phase transformations [19, 20]. The phase diagram for this system is given in Figure 2.8. The most popular specific composition in this system is $0.9Pb(Mg_{1/3}Nb_{2/3})O_3–0.1PbTiO_3$, which is containing 90% PMN and 10% PT, thus increasing the T_m (the temperature of maximum dielectric constant for relaxors, equivalent to T_c for normal ferroelectrics) of PMN to ~40°C. For this composition, the temperature of depolarization (T_d) is ~10°C; hence, the material is a relaxor at room temperature (25°C). An addition of ~28% PT causes the material to revert to a normal ferroelectric tetragonal phase with $T_c \approx 130$°C [2].

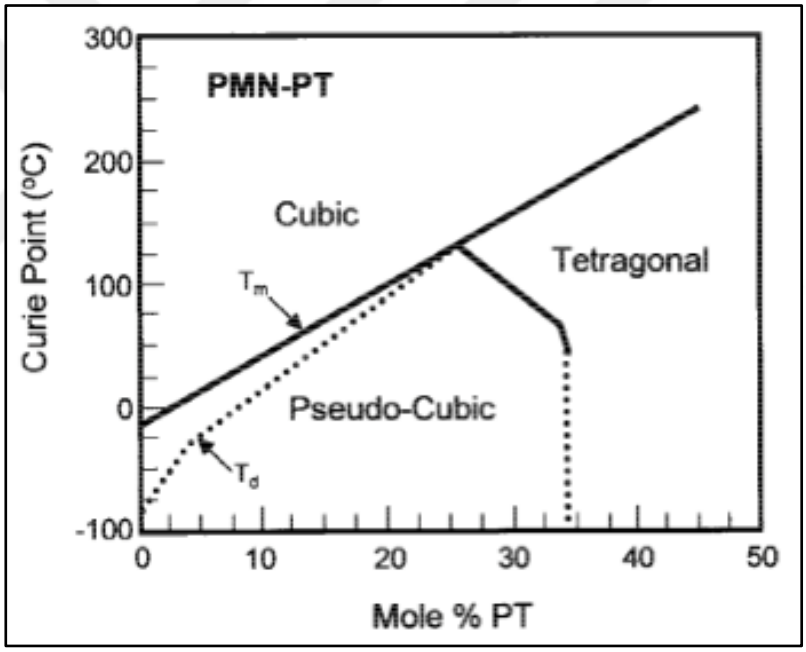

Figure 2.8: Phase diagram of PMN-PT system.

2.6. Grain Orientation Techniques in Electroceramic Materials and Textured Ceramics

Besides the crystal structure and composition, the microstructure plays a decisive role in the physical properties of ceramics. Microstructure is a concept that covers the grains, pores and grain boundaries. The main microstructure properties are particle size and distribution, pore density, pore size and regions. The direction of the

crystal axes of each grain determines its characteristic. The grain arrays of a sintered ceramic material are usually random. The crystalline axes are deliberately called ceramic materials, which are directed by a number of techniques [21].

Most properties of the crystal depend on the orientation of the crystal axes and can be measured. The physical properties measured in a sintered ceramic are averages of randomly aligned beads and in many cases less than single crystal material. Texturalized ceramics behave very close to the single crystal due to the alignment of the crystal axes in the same direction. The physical properties are also naturally affected by this situation.

So far, both in the literature and industrially, production techniques used for the production of such a microstructure are collected under two main headings. The first one is the creation of a grain structure perpendicular to the direction of the force by applying a uniaxial force at high temperature [22]. The resulting anisotropic grains are thus obtained after sintering. This method is called hot forging or hot pressing [21]. The implementation of these regulations is not very advantageous due to high production costs, high density and desired composition, and difficulties in the production of large parts [23].

The second method used to create the texture structure is to direct the sludge containing the anisotropic template parts during the production of the wet material by means of the shear force (Tape casting, extrusion etc.) [22]. These techniques can be divided into 4 groups in general terms;

- Orientation of anisotropic parts by forming (OCAP),
- Template grain growth (TGG),
- Reactive-templated grain growth (RTGG).
- Heterogeneous template grain growth (heterotemplated grain growth, HTGG) [21].

2.6.1. Template Grain Growth (TGG)

TGG technique allows the production of ceramic materials close to the properties of a single crystal with textural structure. It is almost identical to OCAP. The only difference between them is the use of a mixture of coaxial and anisotropic

needles in the TGG method. High-textured ceramics, such as PMN-PZT, PMN-PT and NBT, are produced using the template-augmentation method. These materials have similar piezoelectric properties in the single-crystal direction in the textured direction, and by applying this technique to piezoelectric ceramics, a structure with preferentially growing and oriented grains is obtained. In reducing the cost of single crystal-like materials, the TGG method has a significant contribution in the production of simple or complex geometries in the process of forming high-volume and low-cost conventional ceramics [24].

Large and needle-like template is dispersed in the matrix in which the parts of the coaxial parts. Each of these template particles is single crystal and the nucleation-growth takes place on these particles. However, the thermal and crystallographic properties of the template particles used must be similar to the matrix. Initially, these parts are positioned randomly in the suspension. However, by means of production methods such as tape casting and extrusion, directionality is formed by cutting and shaping. During sintering, the preferred growth occurs on the oriented parts and the oriented grains are obtained [23].

3. EXPERIMENTAL STUDY

3.1. Synthesis and processing of 0.9PMN-0.1PT Powders and Dry-Pressed Ceramics

In this experimental study, the chemicals used for the preparation of 0.9PMN-0.1PT powder synthesis and bulk ceramics are described in detail in Table 3.1,

Table 3.1: Properties of chemicals used in powder synthesis.

Chemical	Aim of Use	Commercial Source	Purity (%)	CAS No.
$(MgCO_3)_4Mg(OH)_2.5H_2O$	$MgNb_2O_6$	Alfa Aesar	99	56378-72-4
Nb_2O_5	Synthesis	Alfa Aesar	99	1313-96-8
$C_2H_2O_8Pb_3$		Sigma Aldrich	99	1319-46-6
TiO_2	PMN-PT	Degussa,P25	99.9	13463-67-7
TiO_2	Powder	Alfa Aesar	99	13463-67-7
PbO	Synthesis	ZAG	99.9	1317-36-8
PbO		Alfa Aesar	99.9	1317-36-8
Polyvinyl Butrial (PVB)		Sigma Aldrich	-	63148-65-2
Polyethylene Glycol (PEG)	Binder	Fluka	-	25322-68-3
Benzyl butyl phthalate (BBP)		Sigma Aldrich	-	85-68-7

0.9PMN-0.1PT powders were prepared by the Columbite method to eliminate the secondary phases that may occur after calcination [4]. In this respect, it is one of the leading components for 0.9PMN-0.1PT powders. Magnesium niobate ($MgNb_2O_6$) was synthesized using $(MgCO_3)4Mg(OH)_2.5H_2O$ and Nb_2O_5. If the preparation of the 0.9PMN-0.1PT powders by the solid state calcination method is synthesized by the direct use of MgO, which is used as the starting powder, forming of the secondary phases after the calcination process could not be eliminated. So, $MgNb_2O_6$ is firstly synthesized for this study. The synthesis of $MgNb_2O_6$ and 0.9PMN-0.1PT powders were given in details in the flow chart shown in Figure 3.1.

The powders weighed at the appropriate stoichiometric ratios according to Equation 3.1 were mixed in a plastic bottle at a speed of 140 rpm in a ball mill for 24 hours in ethanol by using Y_2O_3 stabilized ZrO_2 balls with 3 and 5 mm diameters.

$$(MgCO_3)Mg(OH)_2.5H_2O + 5Nb_2O5 \rightarrow 5MgNb_2O_6 + 4CO_2 + 6H_2O \quad (3.1)$$

The ball-mill was used for the mixing and grinding processes during the synthesis of powders. Mixing and grinding of the powders were made in the ball-mill and it was dried until the slurry consistency in the magnetic stirrer and held in the oven at 80°C for 24 hours. So that the grain size was reduced. The preparation steps of the 0.9PMN-0.1PT powders, as named Powder I and Powder II, were indicated in Equation 3.2 and 3.3, respectively. The stoichiometric amounts of $MgNb_2O_6$, PbO and TiO_2 (Alfa Aesar/Rutile phase) were mixed for Powder I. The stoichiometric amounts of $MgNb_2O_6$, $C_2H_2O_8Pb_3$ and TiO_2 (Degussa/Rutile-anatase phases) were mixed for Powder II. Both of the powders (Powder I and Powder II) were weighed and mixed in a ball mill in ethanol medium for 24 hours, separately.

$$PbO + 0.3MgNb_2O_6 + 0.1TiO_2 \rightarrow 0.9Pb(Mg_{1/3}Nb_{2/3})O_3\text{-}0.1PbTiO_3 \quad (3.2)$$

$$0.33C_2H_2O_8Pb_3 + MgNb_2O_6 + 0.1TiO_2 \rightarrow 0.9Pb(Mg_{1/3}Nb_{2/3})O_3\text{-}0.1PbTiO_3 + 0.66\,CO_2 + 0.33H_2O \quad (3.3)$$

After drying, PMN-PT Powder I and Powder II were calcined in Al_2O_3 crucibles for 4 hours at 800-850°C, respectively. In order to prevent lead loss during sintering, 2% by weight of PbO was added and the drying process was applied. The flow chart of the synthesis of 0.9PMN-0.1PT dry-pressed ceramics was shown in Figure 3.2. PVB, PEG and BBP are specified in Table 3.1. The polymeric based binder was prepared by using these chemicals. The binder was put into a bottle with the amount of 7.28% weight of 0.9PMN-0.1PT powder. 0.9PMN-0.1PT powder and methyl ethyl ketone solution were mixed in a bottle and ball-milled for 24 hours. The powders were dried in a magnetic stirrer to keep them from moisture, and the powders passed through a 90 μm stainless steel sieve were granulated. Each powder composition was pressed with a pressure of 80 MPa in a stainless steel mold of 15 mm diameter by weighing approximately 1.2 g. The polymeric based binder in the pellets was removed from the structure in furnace with an output rate of 1°C/min for 30 minutes at 250°C, 30 minutes at 275°C and 60 minutes at 600°C. When the literature studies of 0.9PMN-0.1PT ceramics were examined, it was determined that the appropriate sintering temperature was 1150°C and the thesis study was directed with these procedure [25]. The sintering process was carried out in a tube furnace at 1150°C during 2, 4 and 6 hours for dry-pressed samples under atmospheric conditions.

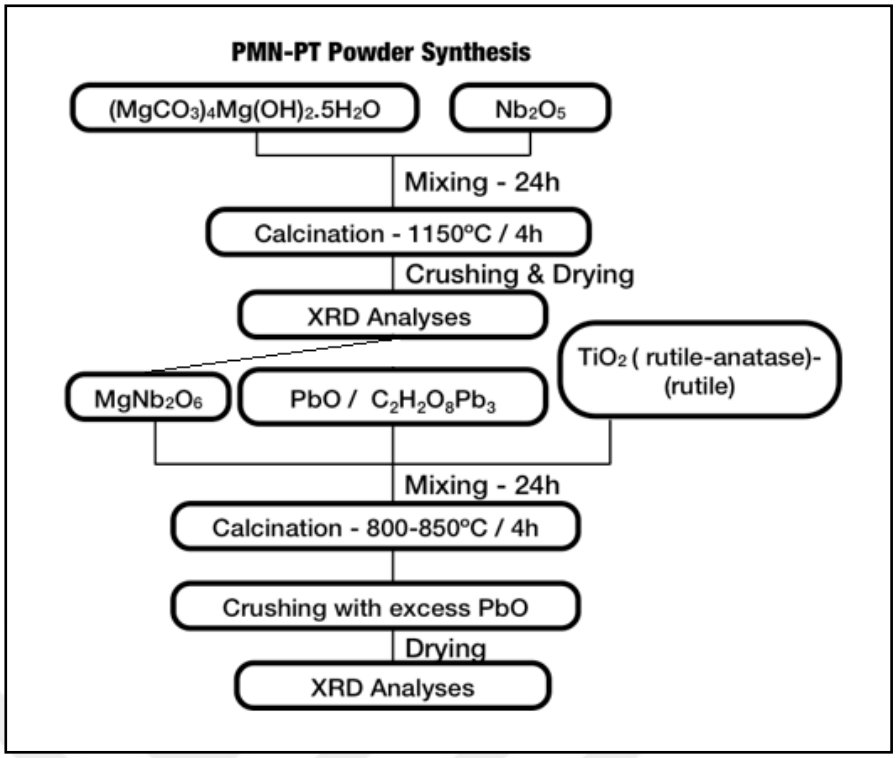

Figure 3.1: The flow chart of $MgNb_2O_6$ and 0.9PMN-0.1PT powders synthesis.

The surfaces must be conductive for the electric field to be applied to the samples. Silver (Ag) electrode is a thin layer on both ceramic disc surfaces, 5°C/min heating speed to 600°C and waiting during 30 minutes for the electrode to hold onto the surface.

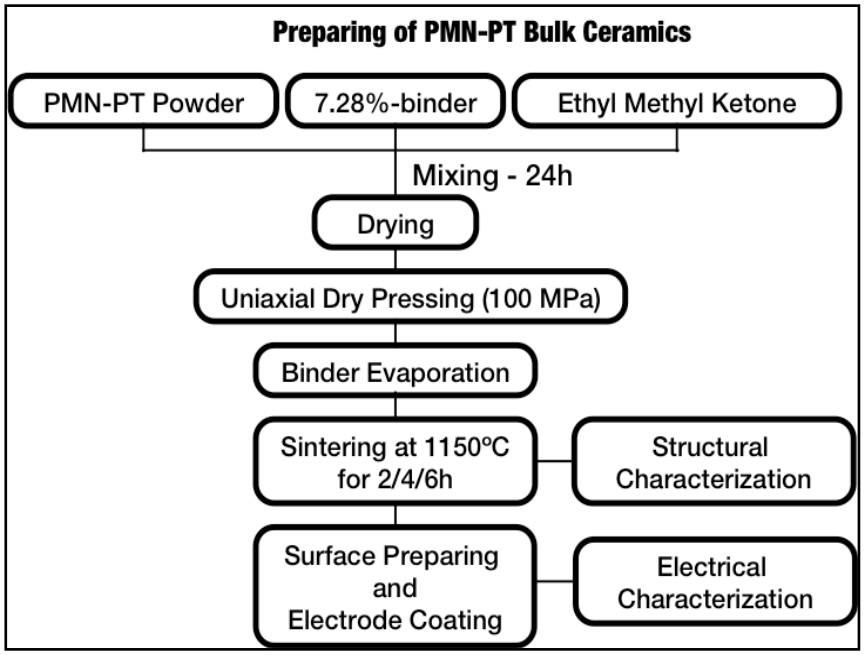

Figure 3.2: The flow chart of preparing 0.9PMN-0.1PT dry-pressed ceramics.

3.2. Characterization of 0.9PMN-0.1PT Ceramics Obtained by Dry-Pressing Method

Firstly, structural characterizations of powders and sintered dry-pressed ceramics were performed. In order to investigate the phase formation, the X-ray diffraction device (Rigaku D/max 2200, Tokyo, Japan) used Cu-Kα (λ = 1.5405 Å) radiation, with a step range of 0.02° and a scanning speed of 1°/min. in 2θ = 20°-70°. After sintering, in order to observe the changes that occur in the microstructure of the surface of a ceramic and scanning electron microscopy (SEM) of polished cross-sectional surface, the SEM device (Philips XL 30 SFEG, Eindhoven, Netherlands) was used. For SEM analysis from the surface, surface treatments of samples were performed using Atlas brand SiC abrasives with 800, 1200 and 2000 respectively, and polished on the silk felt with a particle size of 3 μm and 1 μm particle size (ALS). Thermal etching was performed to clarify grain boundaires. Thermal annealing was carried out for 30 minutes at 980°C, 170°C below the preferred sintering temperature in order to prevent the lead-loss from the structure at high temperatures. The experimental densities of the sintered samples are based on the open pores and the Archimedes principle. According to this principle; after sintering dry sample weight (W_{dry}), wet sample weight in distilled water (W_{hanger}) and direct wet sample (W_{wet}) are calculated with Equation 3.3.

$$\rho_{experimental} = \frac{W_{dry}}{W_{wet} - W_{hanger}} x \rho_{water} \tag{3.3}$$

For electrical characterization, ferroelectric test system (Precision LC, Radiant Inc., Albuquerque, NM) was used for the determination of maximum polarization P_{max}, remnant polarization P_r and coercive field E_c values of piezoceramics depending on the electric field. Electric field-induced strain (S-E) behavior in the samples depending on the applied electric field was measured with the photonic sensor device (MTI-2000, MTI Instruments, Albany, NY), which works in conjunction with the ferroelectric tester. The variation of the dielectric constants (K) and the tanδ values according to the temperature was determined by using the LCR meter for the frequency values of 1, 10, 100 kHz up to 150°C starting from room temperature. Inductance-Capacitance-Resistance (LCR) meter (Hioki 3532-50, Japan) was used for electrical properties of ceramic samples. Hence, Curie

temperature (T_c) was determined. Dielectric constant (K) and dielectric loss (tanδ) of each composition were determined depending on the temperature.

3.3. Processing of Random and Textured 0.9PMN-0.1PT Ceramics Obtained by Tape Casting Method

A systematic calcination study was performed for 0.9PMN-0.1PT powders and the calcination temperature was determined to be 4 hours at 800°C and 850°C. By selecting the lowest calcination temperature without secondary phase, hard lumps were prevented and composition homogenization was achieved. 0.9PMN-0.1PT powders with a general grain size distribution in the range of 0-1 μm were mixed with 43.6% binder and meket solution (66% ethyl methyl ketone-34% ethanol) in the ball mill for 24 h. It is ensured that the casting emulsion taken to the magnetic stirrer is mixed homogeneously with the magnetic fish. At this stage, the non-textured samples of 0.9PMN-0.1PT were prepared with tape casting and the BT template particles without any secondary phase were added at 5% by volume. The emulsion which gets ready for tape-casting with evaporation of excess added solvent meket, was cast to a glass surface by using doctor blade with a speed of 10 cm/s. After drying, the strips cut to the desired dimensions were laminated to approximately 20 times and pressed in the metal mold under pressure of 100 MPa for 3 minutes. The sintering process was carried out in a tube furnace at 1150°C during 4, 6 and 10 hours for textured and non-textured samples under atmospheric conditions. The surfaces must be conductive for the electric field to be applied to the samples. Silver (Ag) electrode is a thin layer on both ceramic disc surfaces, 5°C/min heating speed to 600°C and waiting during 30 minutes for the electrode to hold onto the surface.

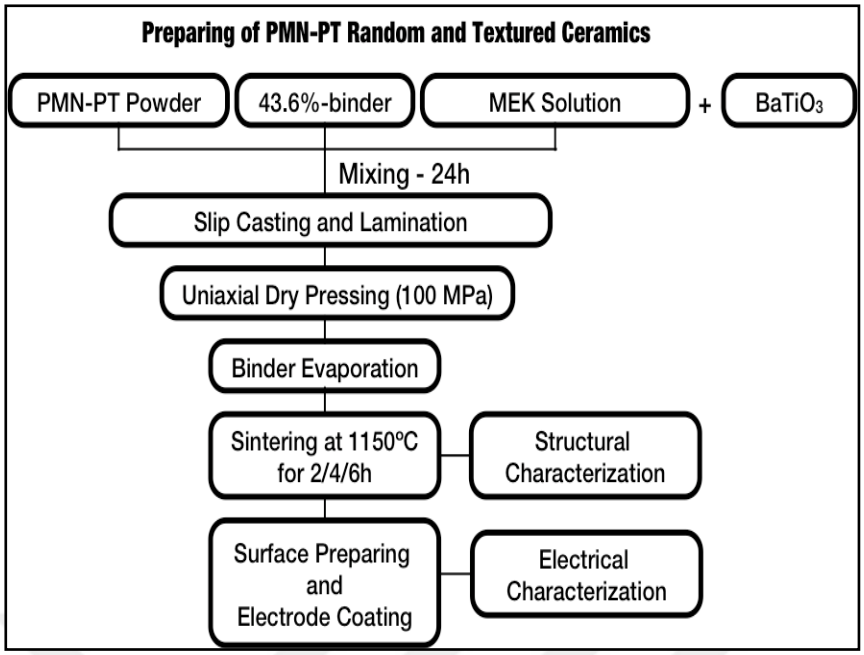

Figure 3.3: The flow chart of preparing 0.9PMN-0.1PT textured with 5% BT and random tape-casted ceramics.

3.4. Characterization of Random and Textured 0.9PMN-0.1PT Ceramics Obtained by Tape Casting Method

Firstly, structural characterizations of powders and sintered dry-pressed ceramics were performed. In order to investigate the phase formation, the X-ray diffraction device (Rigaku D/max 2200, Tokyo, Japan) used Cu-Kα (λ = 1.5405 Å) radiation, with a step range of 0.02° and a scanning speed of 1°/min. in 2θ = 20°-70°. After sintering, in order to observe the changes that occur in the microstructure of the surface of a ceramic and scanning electron microscopy (SEM) of polished cross-sectional surface, the SEM device (Philips XL 30 SFEG, Eindhoven, Netherlands) was used. For SEM analysis from the surface, surface treatments of samples were performed using Atlas brand SiC abrasives with 800, 1200 and 2000 respectively, and polished on the silk felt with a particle size of 3 μm and 1 μm particle size (ALS). Thermal etching was performed to clarify grain boundaires. Thermal annealing was carried out for 30 minutes at 980°C, 170°C below the preferred sintering temperature in order to prevent the lead-loss from the structure at high temperatures. The experimental densities of the sintered samples are based on the open pores and the Archimedes principle. Texture ratios were calculated using lotgering factor from XRD analysis in Equation 3.4, 3.5 and 3.6 [26].

$$f_{L(00l)} = \frac{P_{(00l)} - P_0}{1 - P_0} \quad \text{Lotgering Factor} \tag{3.4}$$

$$P_{(00l)} = \frac{\sum I_{(00l)}}{\sum I_{(hkl)}} \quad \text{Textured orientation ceramic} \tag{3.5}$$

$$P_0 = \frac{\sum I_{0(00l)}}{\sum I_{0(hkl)}} \quad \text{Random orientation ceramic of pollycrstalline} \tag{3.6}$$

For electrical characterization, ferroelectric test system (Precision LC, Radiant Inc., Albuquerque, NM) was used for the determination of maximum polarization P_{max}, remnant polarization P_r and coercive field E_c values of piezoceramics depending on the electric field. Electric field-induced strain (S-E) behavior in the samples depending on the applied electric field was measured with the photonic sensor device (MTI-2000, MTI Instruments, Albany, NY), which works in conjunction with the ferroelectric tester. The variation of the dielectric constants (K) and the tanδ values according to the temperature was determined by using the LCR meter for the frequency values of 1, 10, 100 kHz up to 150°C starting from room temperature. Inductance-Capacitance-Resistance (LCR) meter (Hioki 3532-50, Japan) was used for electrical properties of ceramic samples. Hence, Curie temperature (T_c) was determined. Dielectric constant (K) and dielectric loss (tanδ) of each composition were determined depending on the temperature.

4. RESULTS AND DISCUSSION

In this section, the parameters such as different powder sources, different fabrication methods, diferrent sintering durations and addition of BT templates on the structural and electrical properties of samples were investigated with various characterization methods. Results were discussed with literature in detail.

4.1 X-Ray Diffraction Results

In this section, structural and crystallographic analyses of powder and samples after calcination and sintering were investigated.

4.1.1 Phase Analysis of $MgNb_2O_6$ Powder

The preparation of the 0.9PMN-0.1PT powders synthesized by the solid state calcination method with the direct use of MgO, which was used as the starting powder, could not eliminate the secondary phases obtained after the calcination process, hence we produced magnesium niobate powder by Columbite method and this powder was calcined at 1150°C for 4 hours [27]. Figure 3.1 shows the X-ray diffraction pattern of $MgNb_2O_6$ without secondary phase, which was the precursor powder in the production of the 0.9PMN-0.1PT. The formation of the pyrochlorine phase was the result of the chemical reaction between lead oxide and niobium oxide [28].

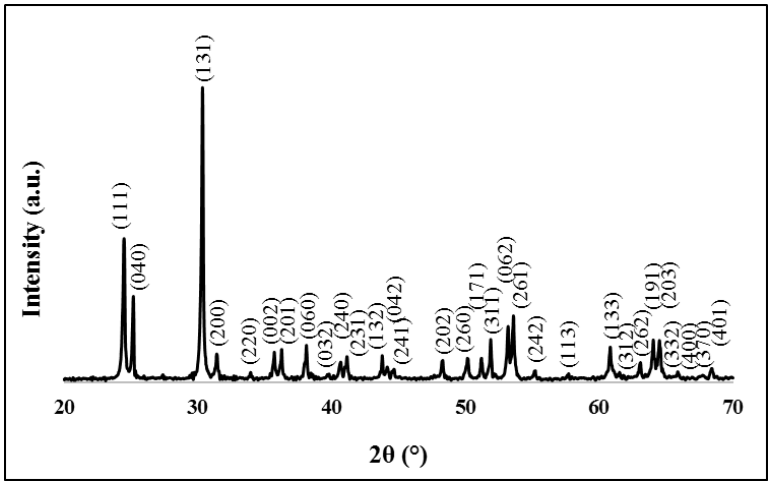

Figure 4.1: The XRD pattern of $MgNb_2O_6$ powder calcined at 1150 °C for 4 h.

4.1.2 Phase Analysis of 0.9PMN-0.1PT Powder

We produced two different types of powders with using lead oxide and lead carbonate and these powders were calcined at different temperatures. X-ray diffraction patterns of 0.9PMN-0.1PT powders calcined at 800°C for powder I and 850°C for powder II for 4 h were shown in Figure 4.2 and Figure 4.4. Both of 0.9PMN-0.1PT powders calcined at these temperatures generally appeared to crystallize in the perovskite structure without any secondary phases (pyrochlore). Pyrochlore is a poor lead phase that exhibits semi-stable and paraelectric properties at certain temperatures in the development of perovskite structure. Since it has a paraelectric character and high conductivity, it is not desirable as a residue in the structure because it negatively affects the electrical properties [29]. In addition, the particle size distribution of the powders which were applied to the crushing process generally varied between 0-1 μm which was shown in Figure 4.3 and Figure 4.5.

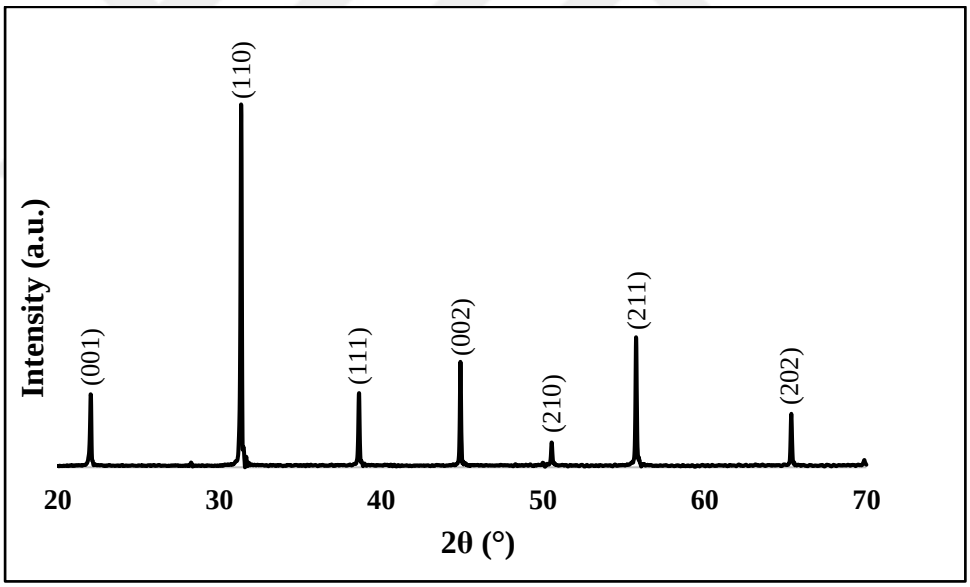

Figure 4.2: The XRD pattern of 0.9PMN-0.1PT powder I calcined at 800°C for 4 h.

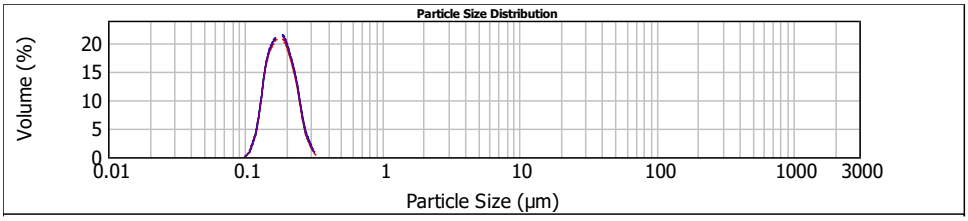

Figure 4.3: The particle size distribution of 0.9PMN-0.1PT powder I calcined at 800°C for 4 h.

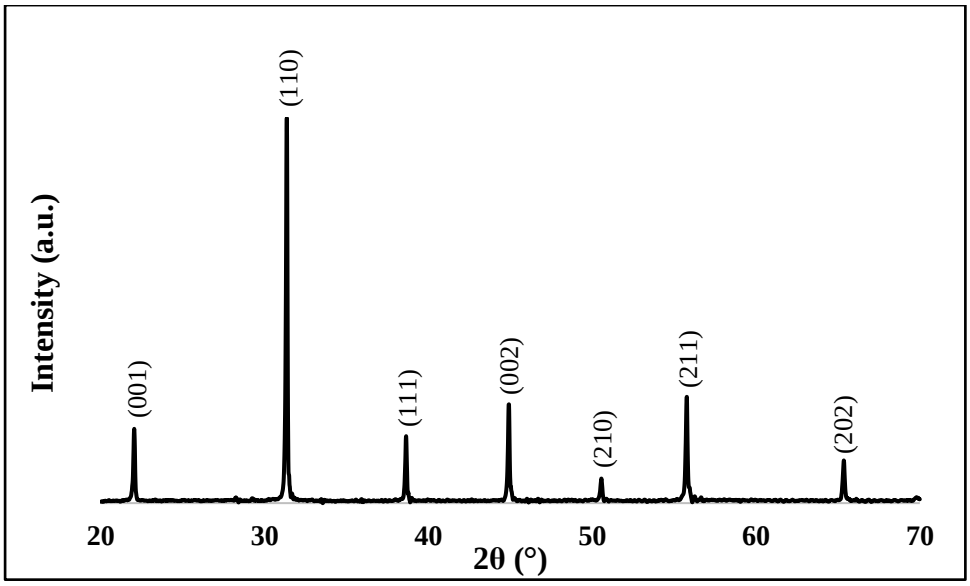

Figure 4.4: The XRD pattern of 0.9PMN-0.1PT powder II calcined at 850°C for 4 h.

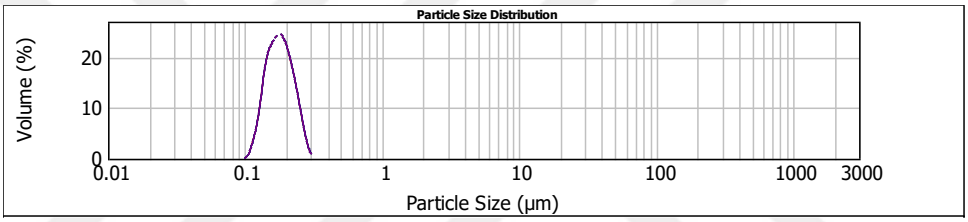

Figure 4.5: The particle size distribution of 0.9PMN-0.1PT powder II calcined at 850°C for 4 h.

The SEM images of powder I and powder II after calcination were shown in Figure 4.6.

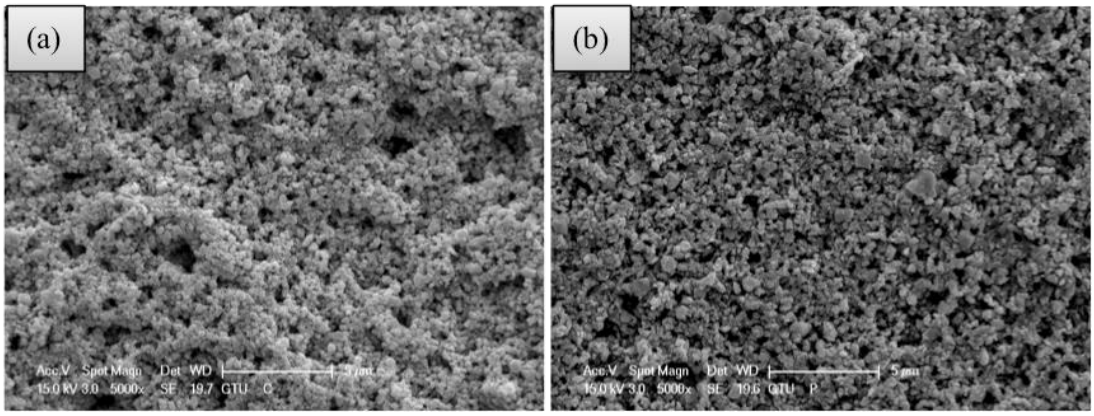

Figure 4.6: SEM images of powders after calcination (a) Powder II (b) Powder I

4.2 Structural Characterization of Dry-Pressed Ceramics

Structural and phase properties of samples produced by using starting powder I and powder II were examined. The comparison of XRD patterns of 0.9PMN-0.1PT dry-pressed ceramics sintered at 1150°C for 2 h, 4 h and 6 h were shown in Figure 4.7 and Figure 4.10. All the samples crystallized in the pure perovskite structure without any secondary phases. The bulk densities of ceramic samples with different sintering durations at 1150°C were measured by Archimedes method. The measured densities were 7.23 – 7.45 g/cm^3, corresponding to 93 – 96% of their theoretical values.

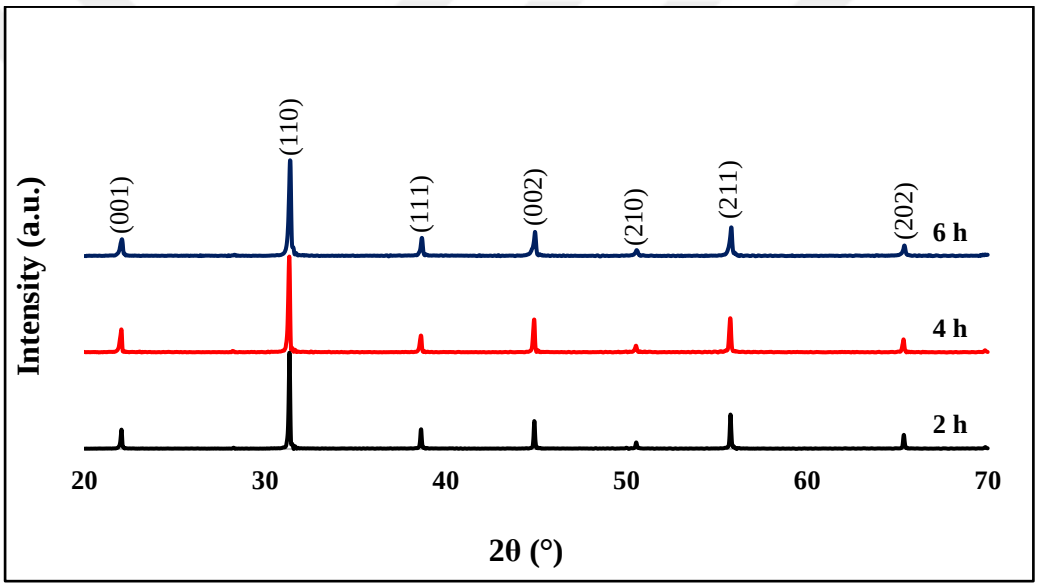

Figure 4.7: The XRD pattern of dry-pressed ceramics produced from starting powder I and sintered at different durations.

SEM micrographs of the thermally etched surface and cross-sectional parts of PMN-PT ceramic samples produced from starting powder I, sintered for different durations were shown in Figure 4.8 and Figure 4.9 respectively. From SEM micrographs, uniform microstructures with sub-micron grains were observed for all ceramic samples. Porosity was decreased with increasing sintering duration.

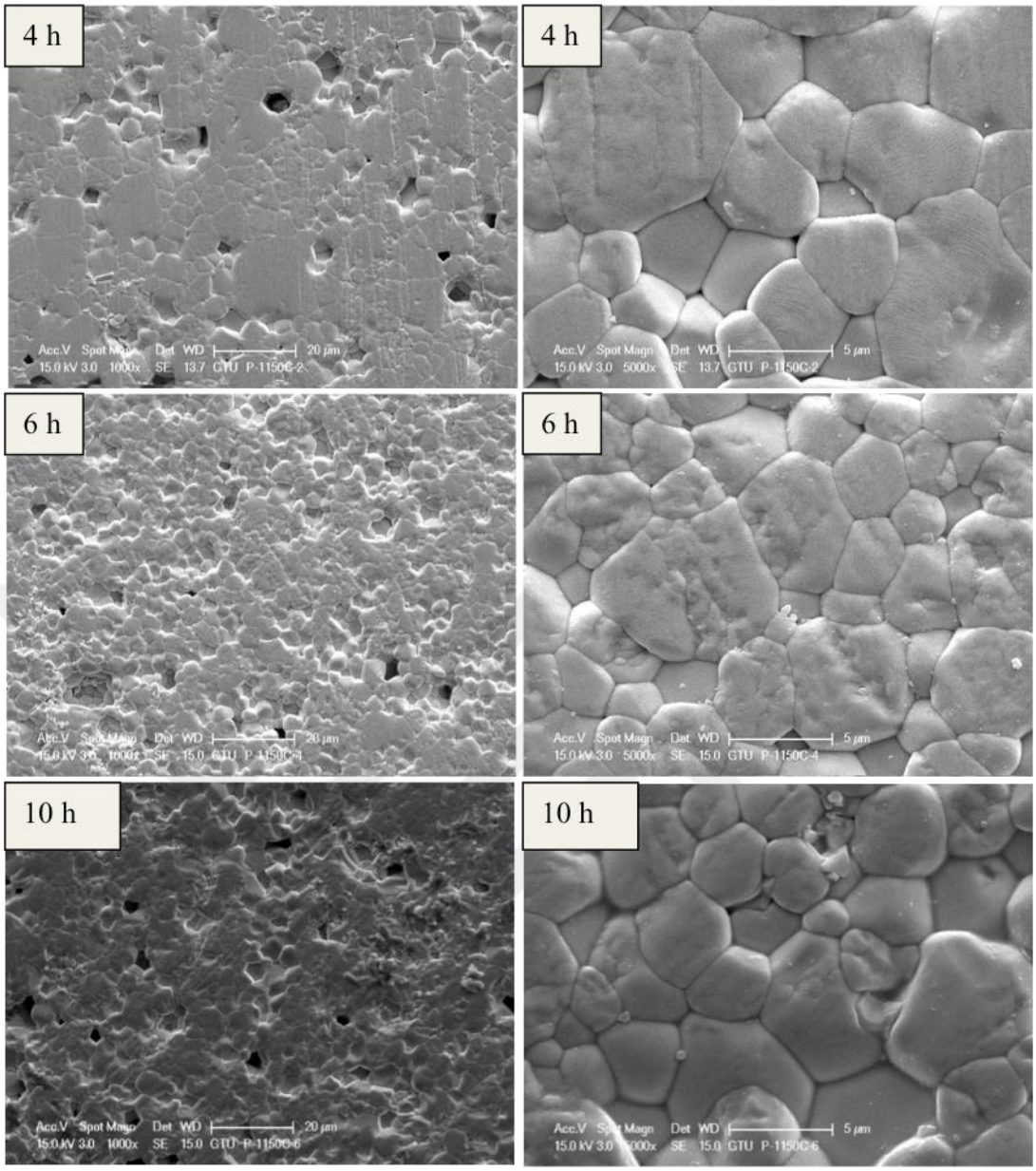

Figure 4.8: The cross-sectional SEM images of dry-pressed ceramics produced from starting powder I and sintered at different durations.

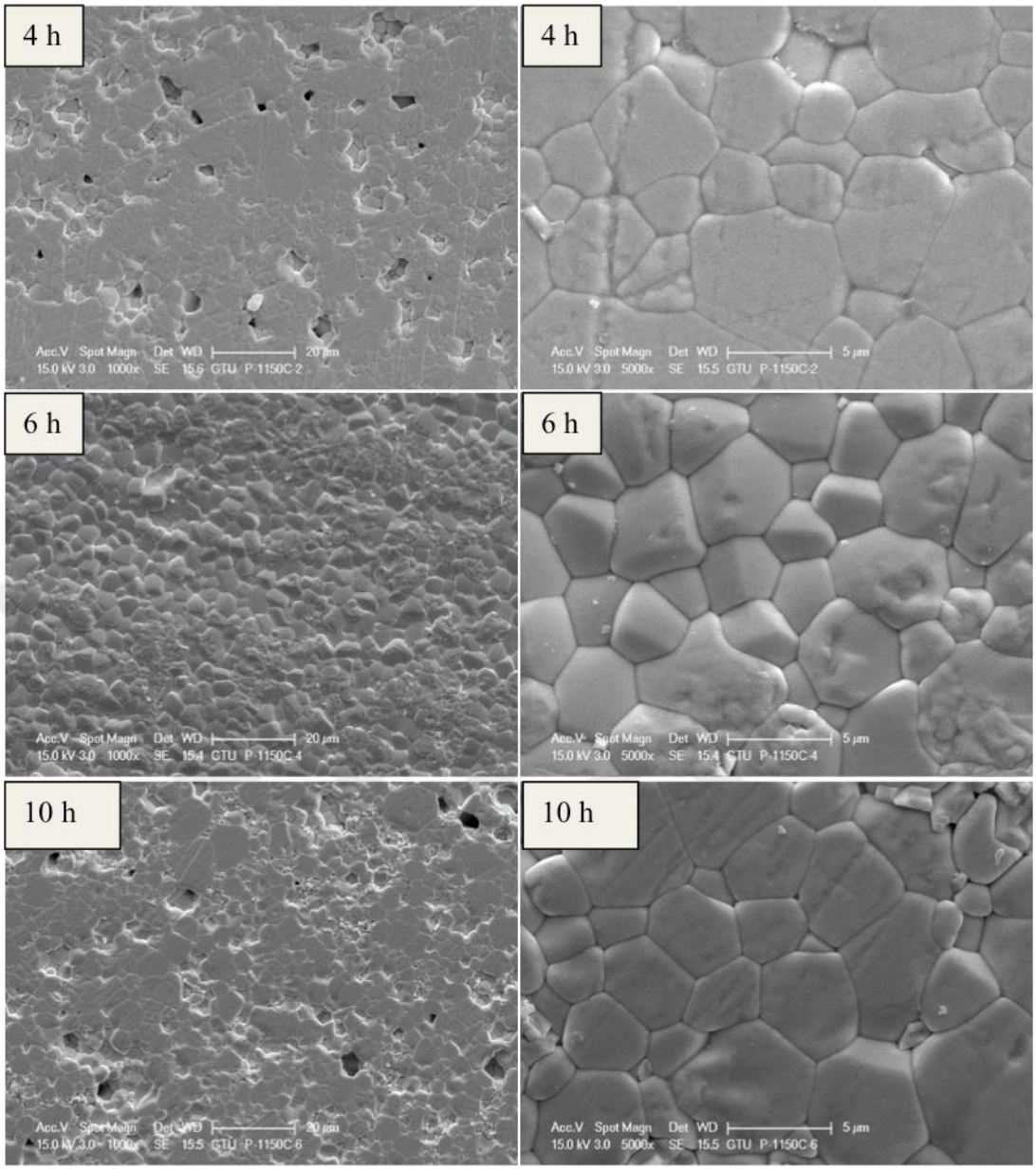

Figure 4.9: The surface SEM images of dry-pressed ceramics produced from starting powder I and sintered at different durations.

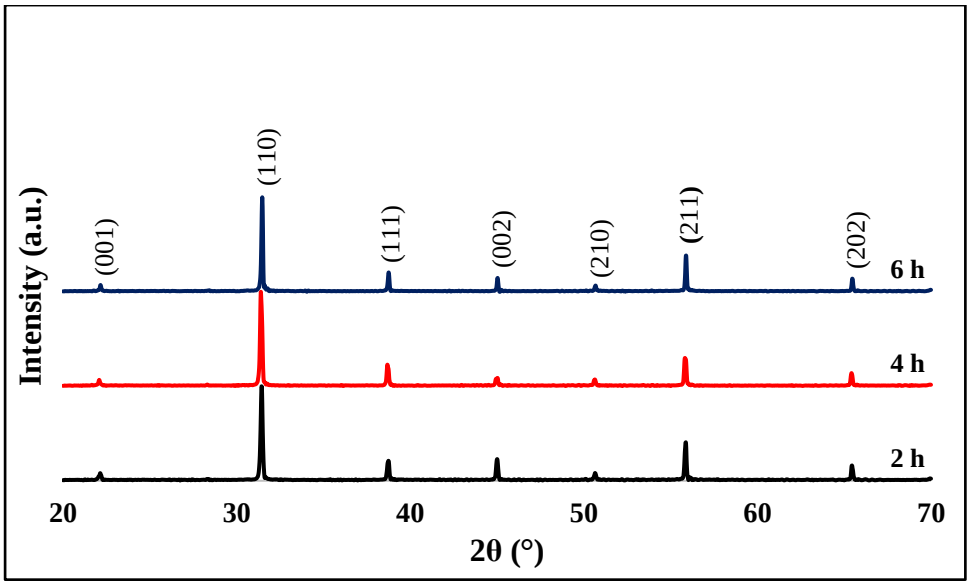

Figure 4.10: The XRD pattern of dry-pressed ceramics produced from starting powder II and sintered at different durations.

SEM micrographs of the thermally etched surface and cross-sectional parts of dry-pressed ceramic samples produced from starting powder II, sintered for different durations, were shown in Figure 4.11 and Figure 4.12 respectively. From SEM micrographs, uniform microstructures with sub-micron grains were observed for all ceramic samples. Porosity is decreased with increasing sintering duration.

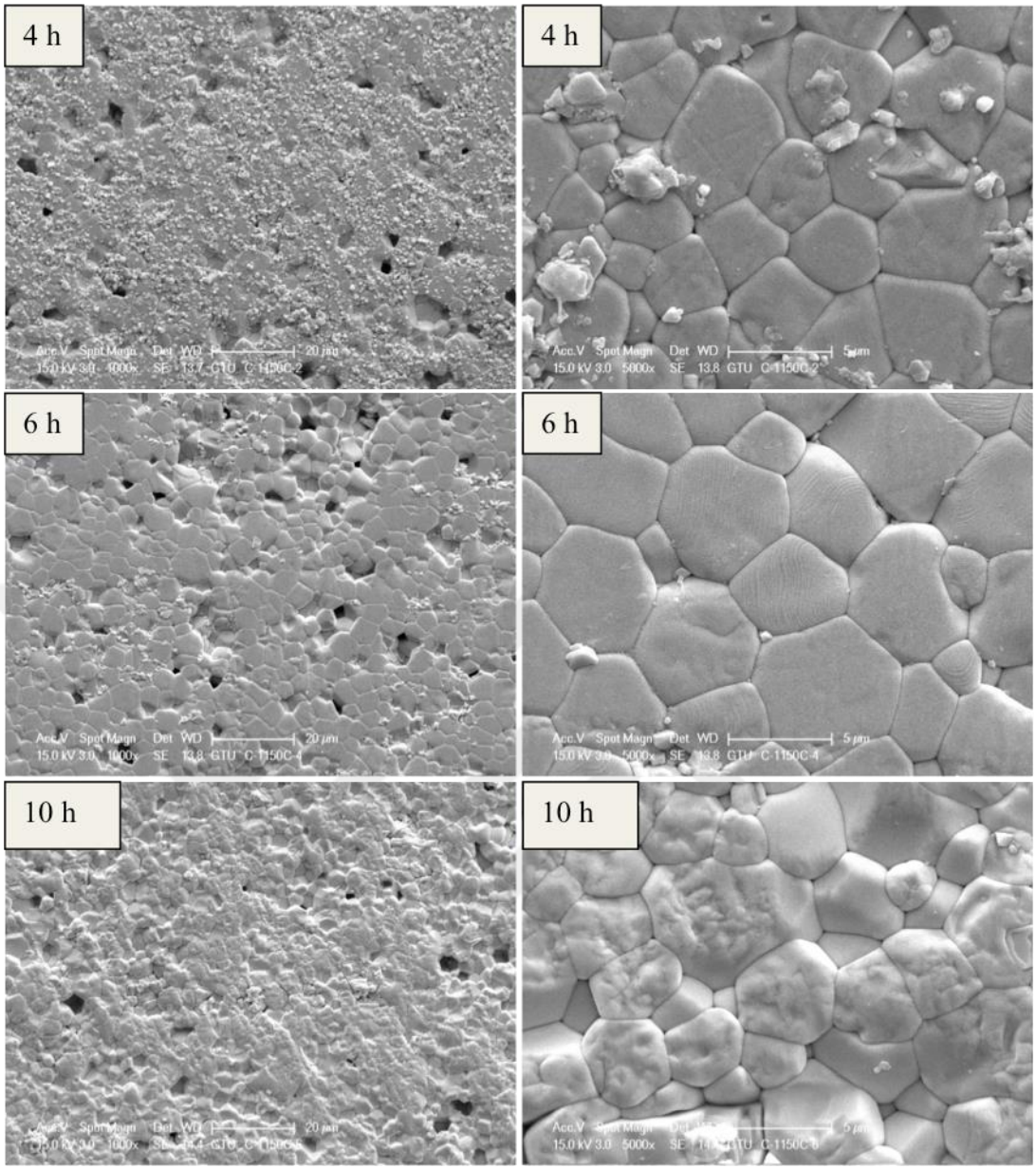

Figure 4.11: The cross-sectional SEM images of dry-pressed ceramics produced from starting powder II and sintered at different durations.

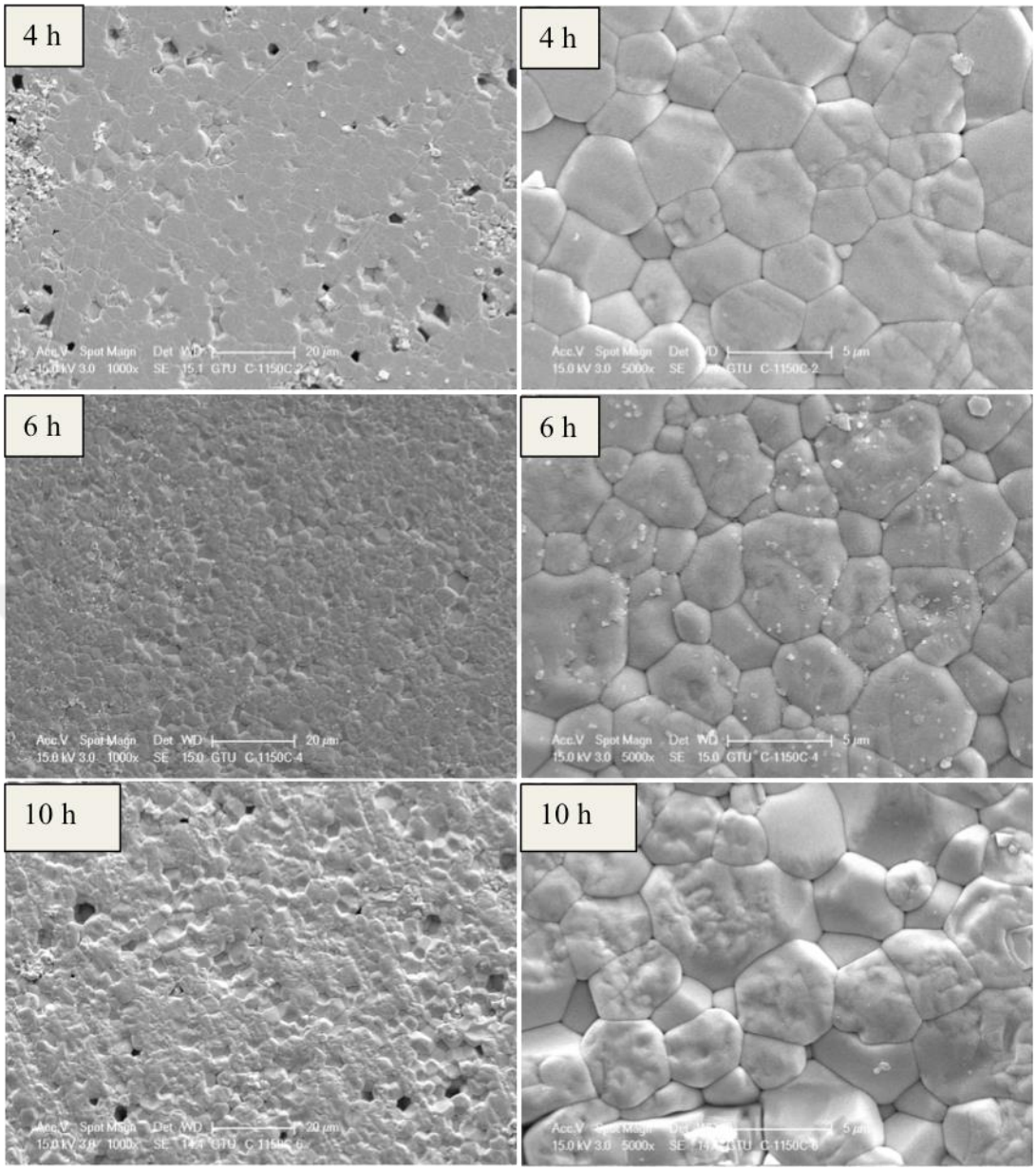

Figure 4.12: The surface SEM images of dry-pressed ceramics produced from starting powder II and sintered at different durations.

4.3 Structural Characterization of Random Tape-Casted Ceramics

Randomly oriented, untemplated samples of matrix composition (2 wt.% excess PbO) were formed in order to directly correlate the effect of processing on the properties. Through this work, the term ‘’random’’ will designate 0.9PMN-0.1PT sample that does not contain $BaTiO_3$ (BT) template particles and the samples display no preferential grain orientation. In tape casting method, the prepared slurry is tape casted, cut and laminated [25]. The random samples were prepared by this method. The X-ray diffraction patterns of random tape-casted ceramics produced from starting powder I and powder II, sintered at 1150°C for 4 h, 6 h and 10 h were shown in Figure 4.13 and Figure 4.16 respectively. All the samples crystallized in the pure perovskite structure without any secondary phases, and slowscan XRD patterns of samples produced from starting powder II, between 44°-46° were also shown in Figure 4.17. There was not peak splitting. This pattern showed that single peak and secondary peak were existed from $CuK_{\alpha 2}$. The densities of all random tape-casted samples with different sintering durations at 1150°C were measured by Archimedes method. The measured densities were 7.8 – 7.85 g/cm^3, corresponding to 95 – 96% of their theoretical values.

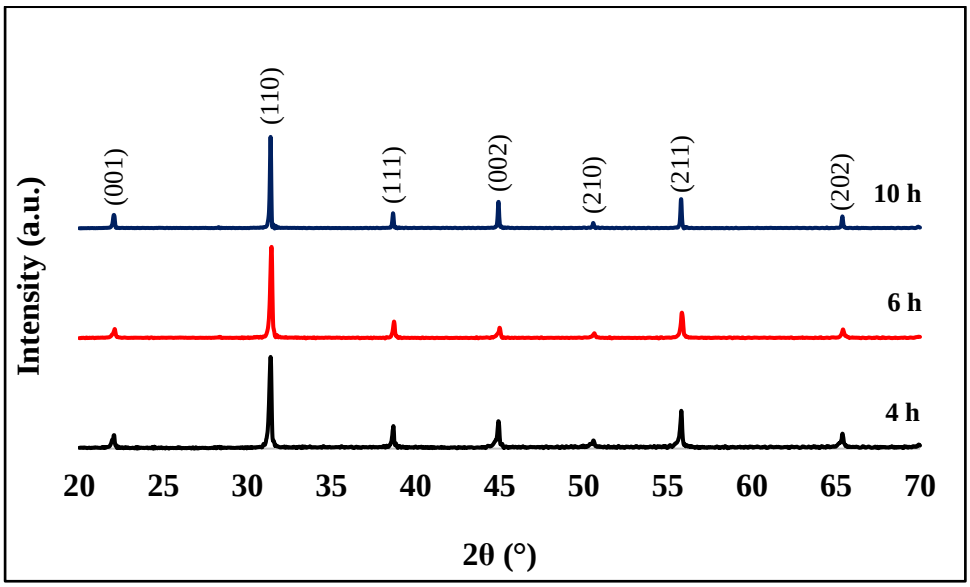

Figure 4.13: The XRD pattern of random tape-casted ceramics produced from starting powder I and sintered at different durations.

SEM micrographs of the thermally etched surface and cross-sectional parts of random tape-casted ceramic samples produced from powder I, sintered for 4 h at 1150°C were shown in Figure 4.14 and Figure 4.15. From SEM micrographs, uniform microstructures with sub-micron grains were observed for ceramic samples.

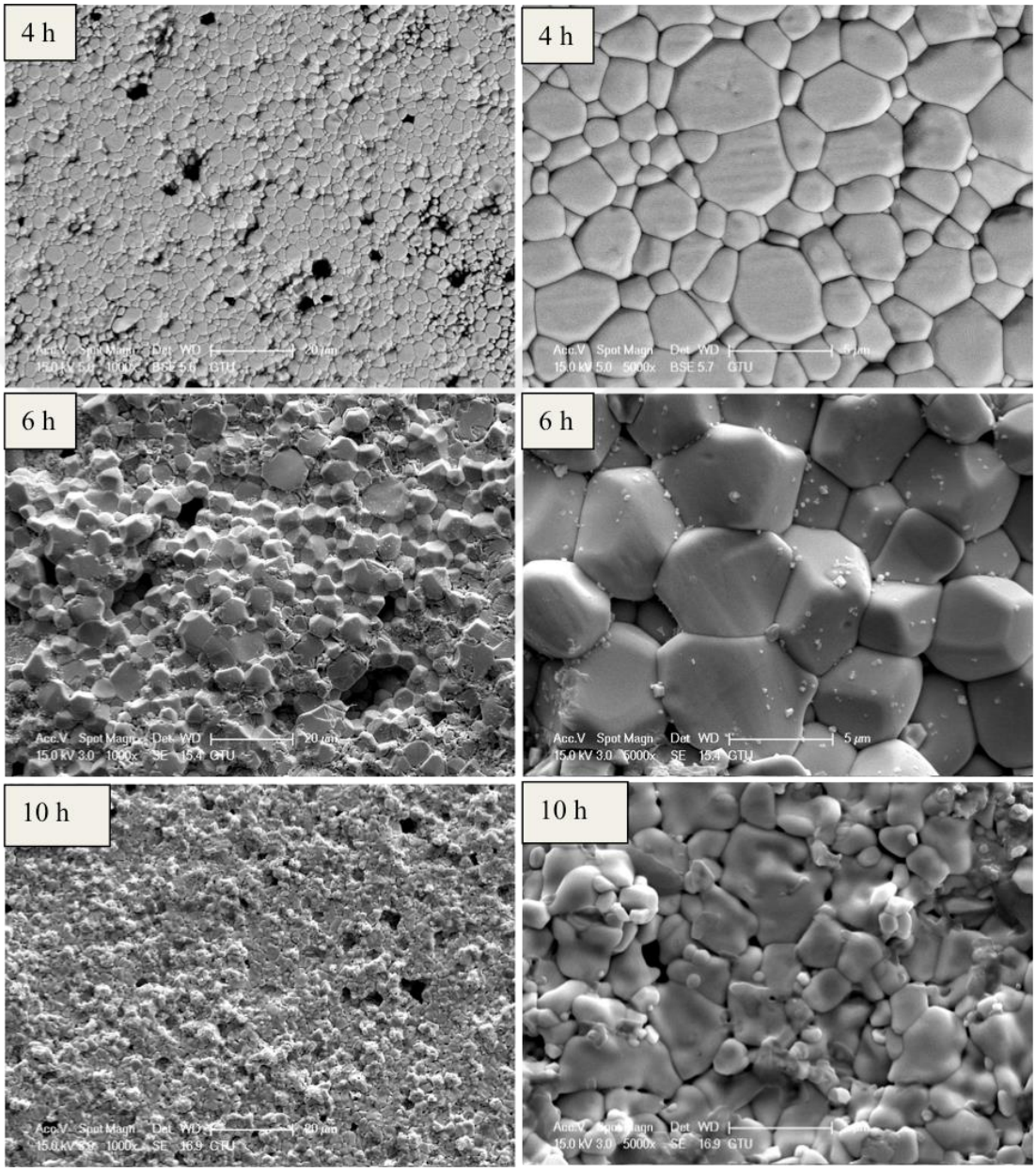

Figure 4.14: The cross-sectional SEM images of random tape-casted ceramics produced from starting powder I and sintered at different durations.

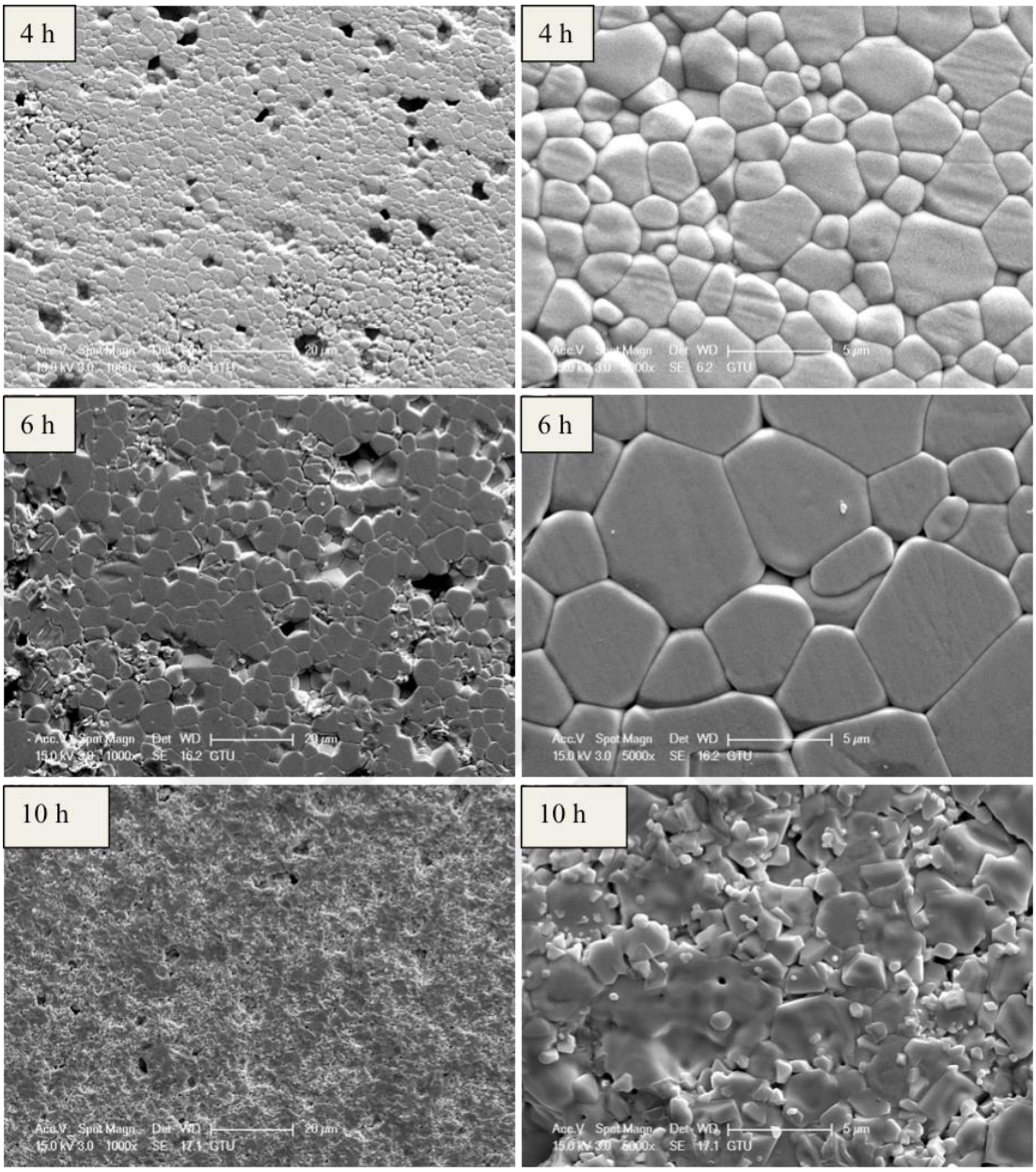

Figure 4.15: The surface SEM images of random tape-casted ceramics produced from starting powder I and sintered at different durations.

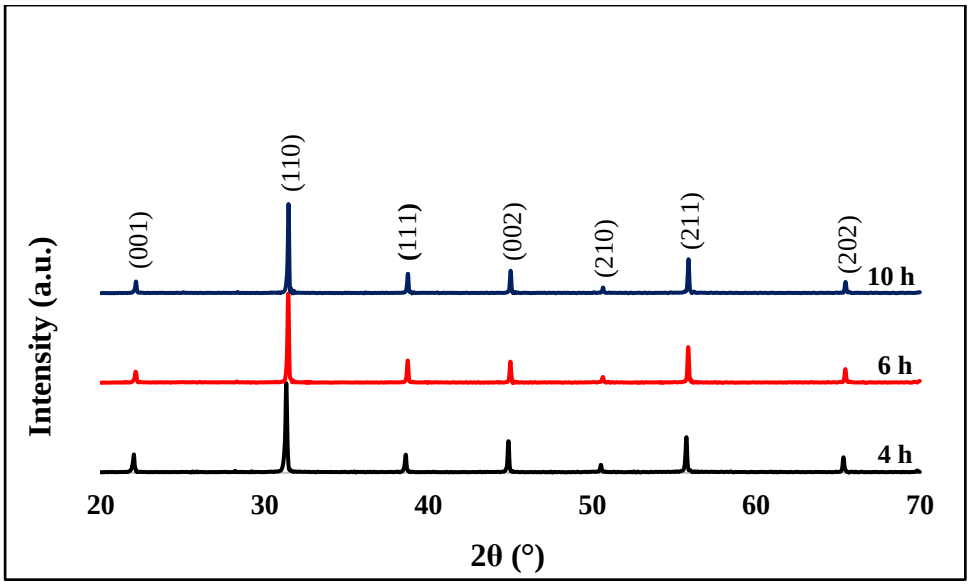

Figure 4.16: The XRD pattern of random tape-casted ceramics produced from starting powder II and sintered at different durations.

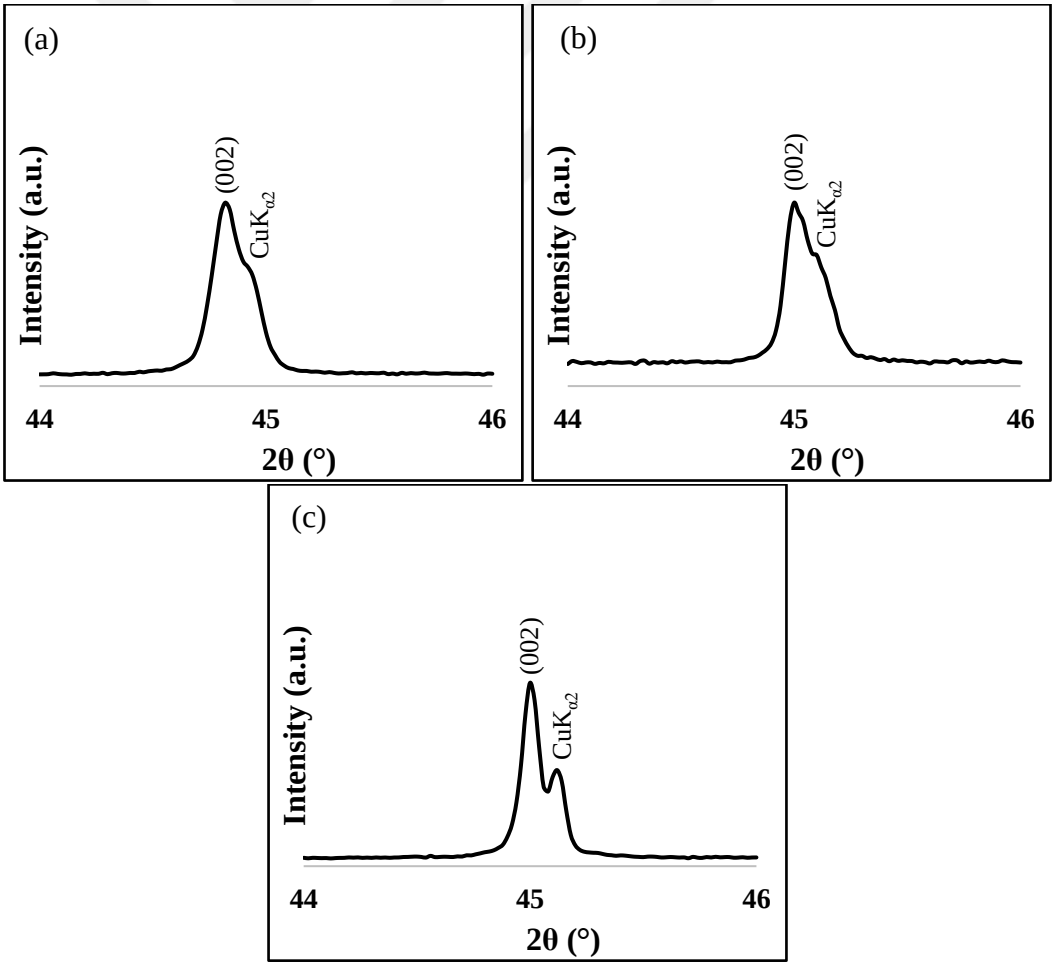

Figure 4.17: The slow scan of (002) peak of random tape-casted ceramics produced from starting powder II and sintered at different durations (a) 4 h, (b) 6 h, (c) 10 h.

SEM micrographs of the thermally etched surface and cross-sectional parts of random tape-casted ceramic samples produced from starting powder II and sintered for different durations, were shown in Figure 4.18 and Figure 4.19 respectively. From SEM micrographs, uniform microstructures with sub-micron grains were observed for all ceramic samples. Porosity was so dominant at all samples.

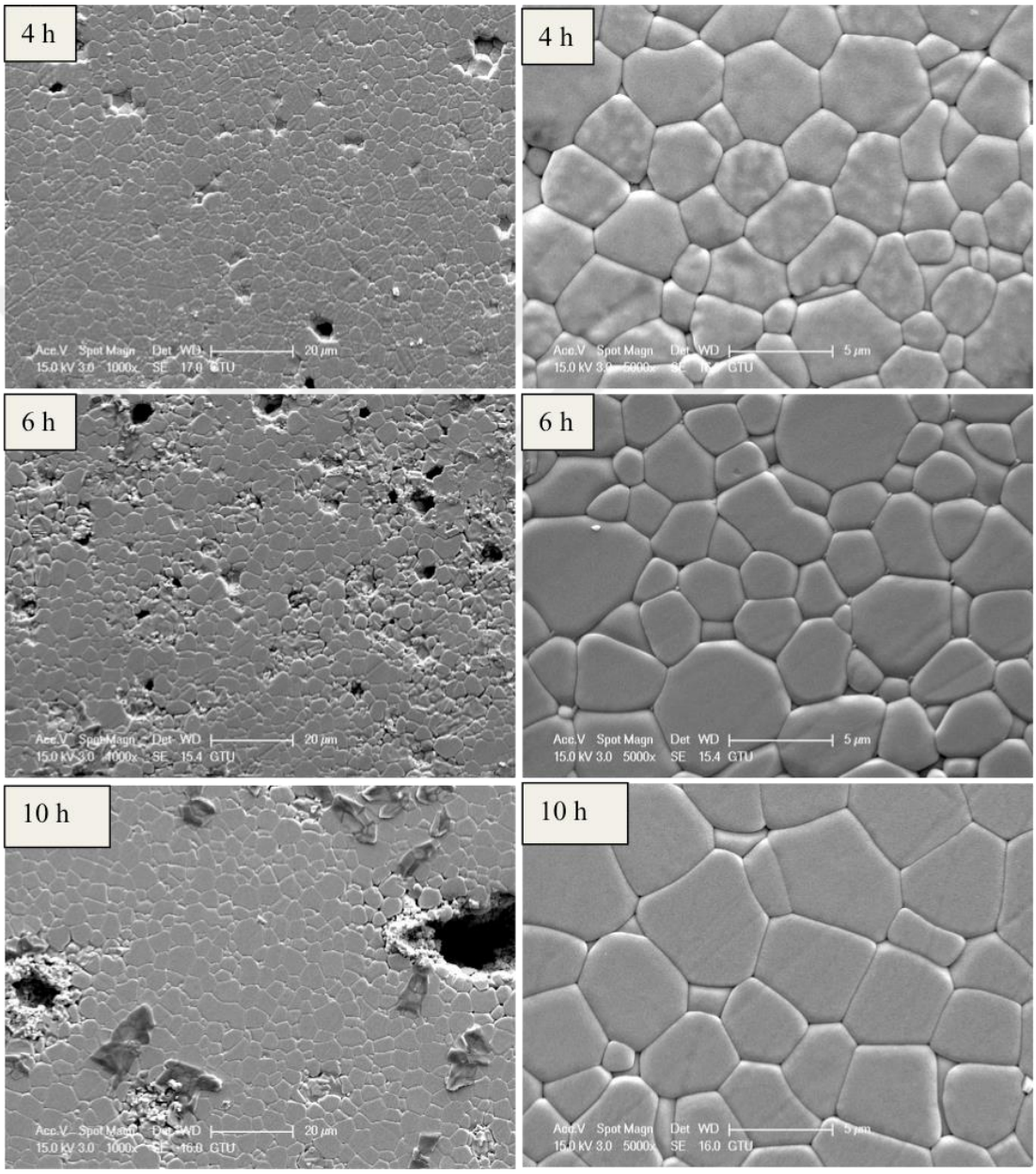

Figure 4.18: The cross-sectional SEM images of random tape-casted ceramics produced from starting powder II and sintered at different durations.

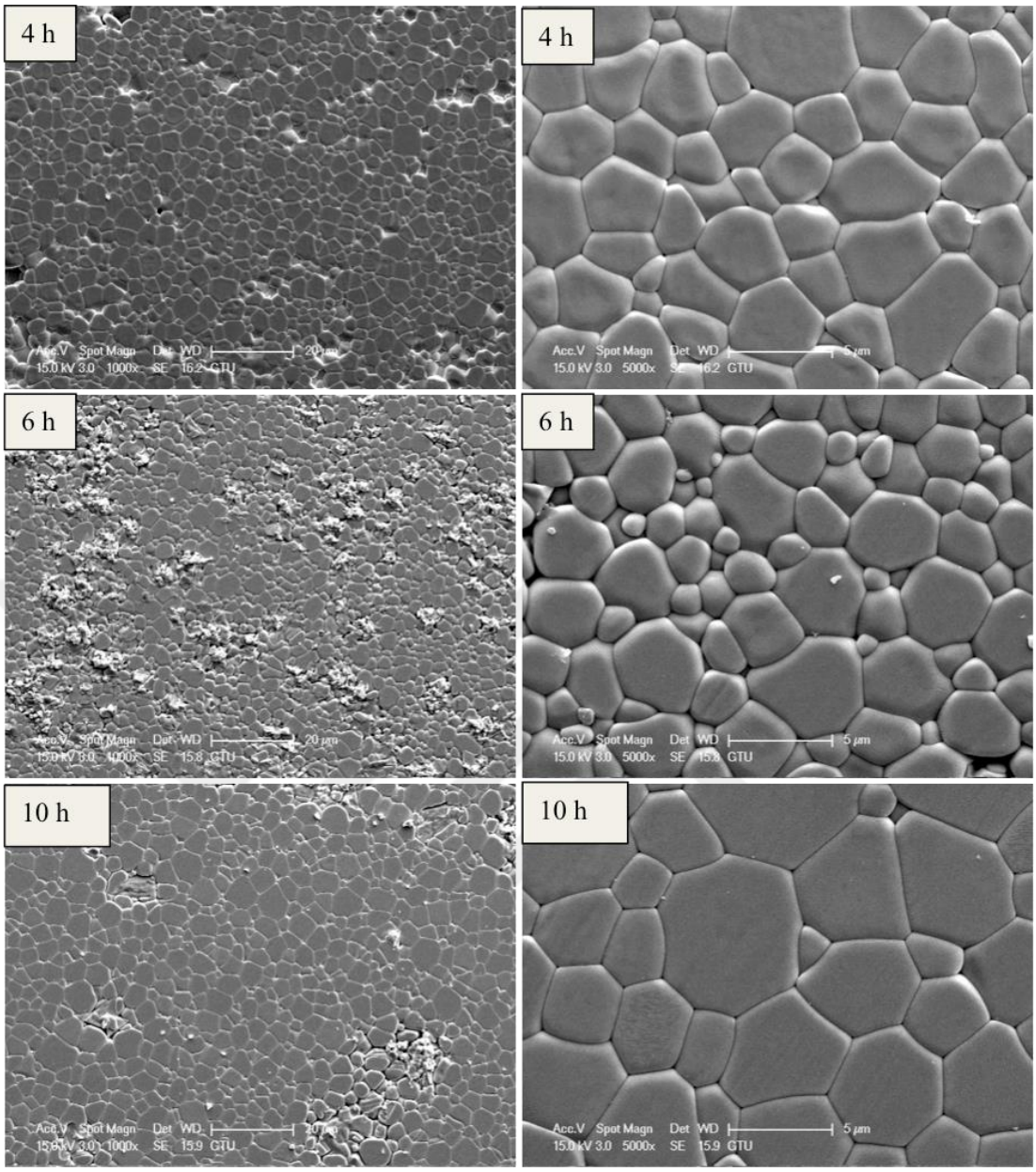

Figure 4.19: The surface SEM images of random tape-casted ceramics produced from starting powder II and sintered at different durations.

4.4. Structural Characterization of Textured Ceramics

BT template was used in the present work. Samples were textured using 5% vol BT templates by tape-casting and TGG methods. Figure 4.20 and 4.23 shows the x-ray diffraction pattern of the textured tape-casted PMN-PT samples. When the x-ray diffraction patterns were examined, any secondary phase formation was not observed. The lotgering factor represent the textured fraction of the samples sintered at 1150°C for 4 h, 6 h and 10 h as shown in Figure 4.20 and Figure 4.23. The texture fractions were 0.74, 0.80 and 0.80. These values were for the samples produced from starting powder II. For the samples produced from starting powder I, the lotgering factor's values were 0.48, 0.54 and 0.54 for 4 h, 6 h, and 10 h respectively. In addition, to prevent lead volatility during sintering 2% excess PbO contribution by weight appeared to be sufficient. The densities of all textured ceramic samples with different sintering durations at 1150°C were measured by Archimedes method. The measured densities were 7.9 – 7.95 g/cm^3, corresponding to 98 – 99% of their theoretical values.

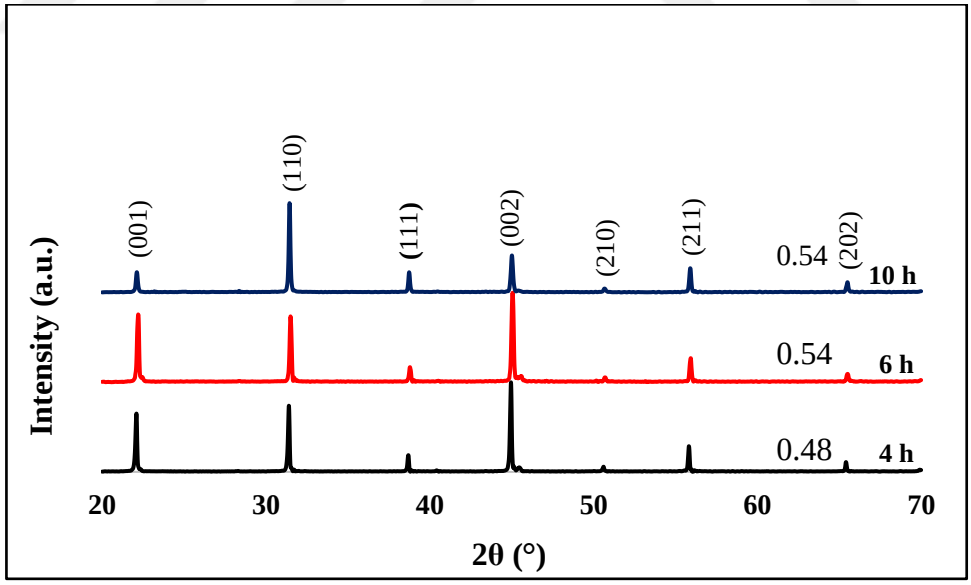

Figure 4.20: The XRD pattern of textured tape-casted ceramics with 5% BT produced from starting powder I and sintered at different durations.

Samples were textured using 5% vol BT templates by tape-casting and TGG methods. This amount was kept as constant BT ratio in the structure. SEM micrographs of the thermally etched surface and cross-sectional parts of 5% BT

textured PMN-PT ceramic samples produced from starting powder I, sintered at 1150°C for different durations, were shown in Figure 4.21 and Figure 4.22. From SEM micrographs, uniform microstructures with sub-micron grains were not observed for all ceramic samples. Adding the BT templates changed the grain size of TGG in PMN-PT ceramics. Grain growth was not equal in all grains of ceramics. The grain of TGG increased, other grains decreased and they were not equal to each other. Grain refining with increasing sintering duration was also observed.

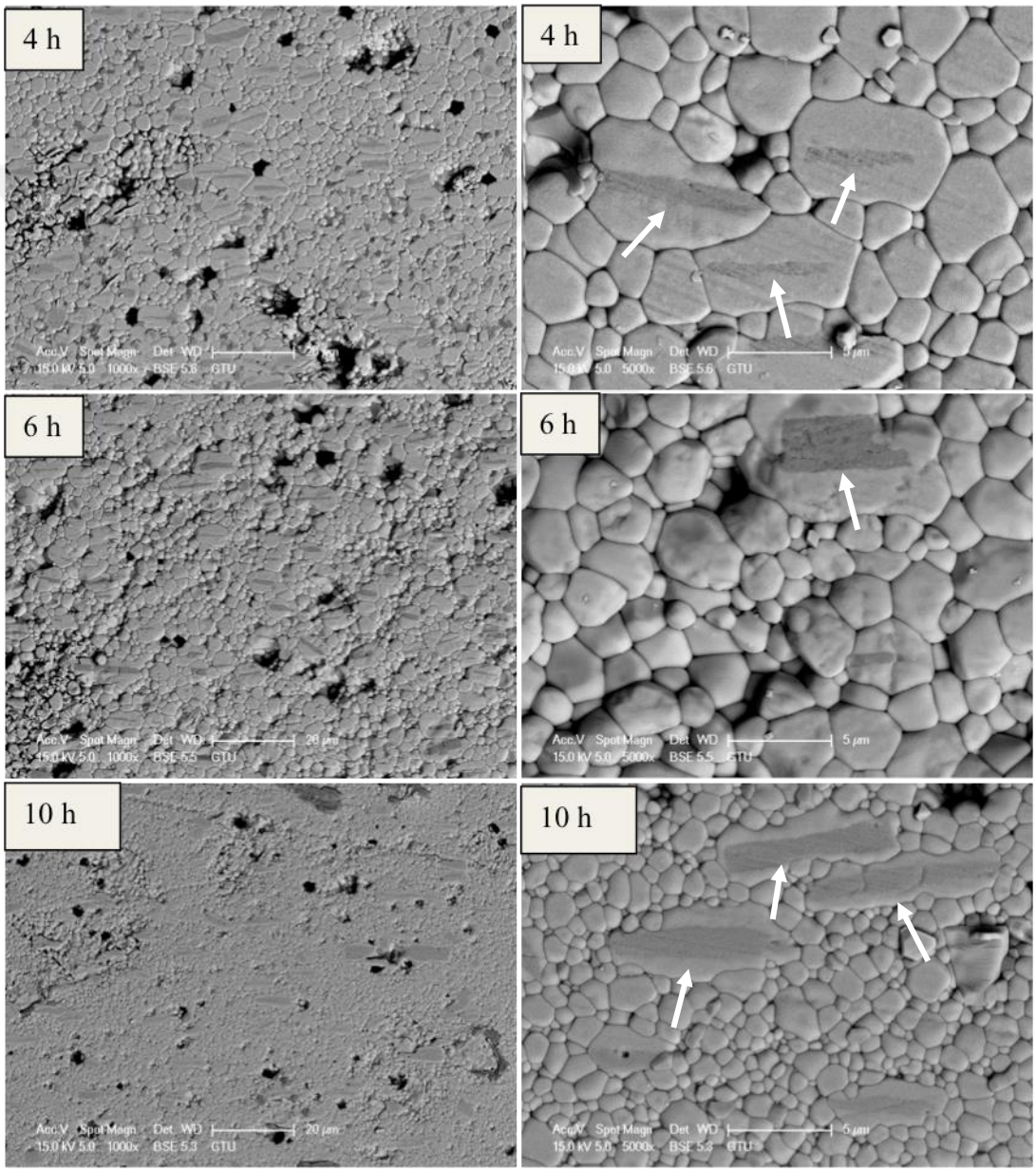

Figure 4.21: The cross-sectional SEM images of textured tape-casted ceramics with 5% BT produced from starting powder I and sintered at different durations.

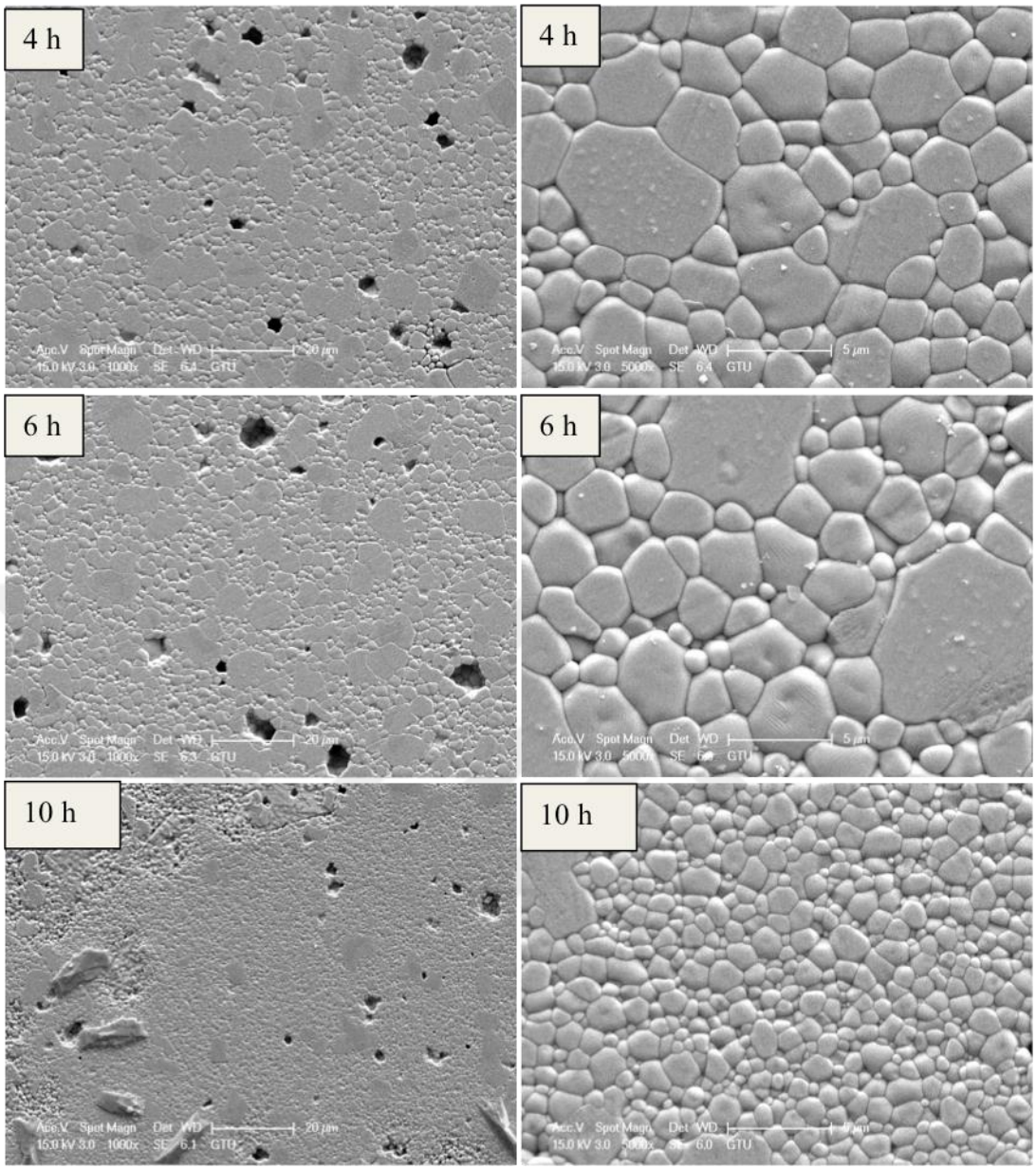

Figure 4.22: The surface SEM images of textured tape-casted ceramics with 5% BT produced from starting powder I and sintered at different durations.

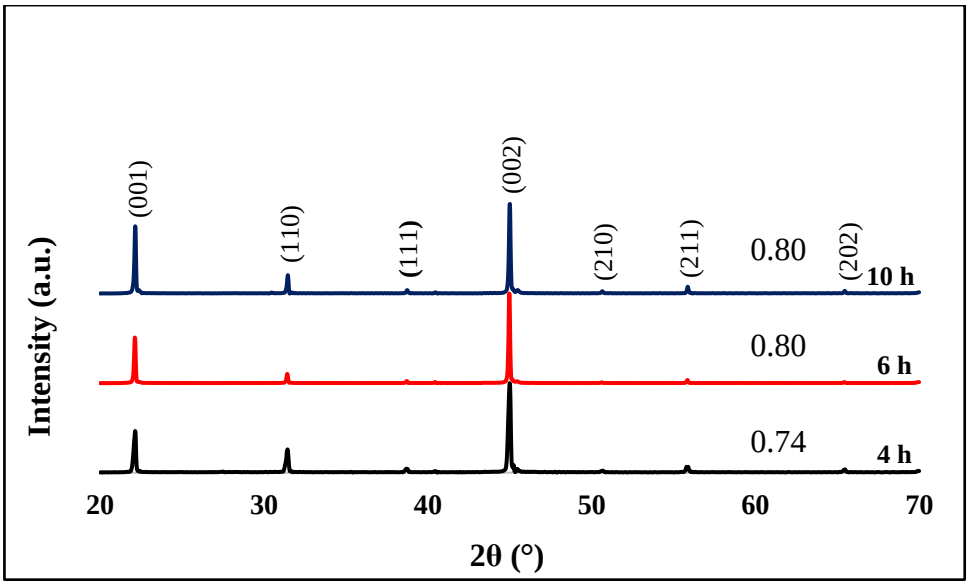

Figure 4.23: The XRD pattern of textured tape-casted ceramics with 5% BT produced from starting powder II and sintered at different durations.

SEM micrographs of the thermally etched surface and cross-sectional parts of 5% BT textured PMN-PT ceramic samples produced from starting powder II, sintered at 1150°C for different durations, were shown in Figure 4.24 and Figure 4.25. From SEM micrographs, uniform microstructures with sub-micron grains were observed for all ceramic samples. Porosity was decreased with increasing sintering duration. Adding the BT templates changed the grain size of TGG in PMN-PT ceramics. Grain growth was equal to each other in all grains of ceramics, and samples exhibited brick wall. The templates were very clearly visible and were found to be well aligned in PMN-PT matrix. The grain size of the samples were measured as ~5 μm. Both surface and cross-sectional views of microstructures indicated a dense ceramic. Grain boundaries were also clearly visible, and identified by white arrows on the micrographs [30].

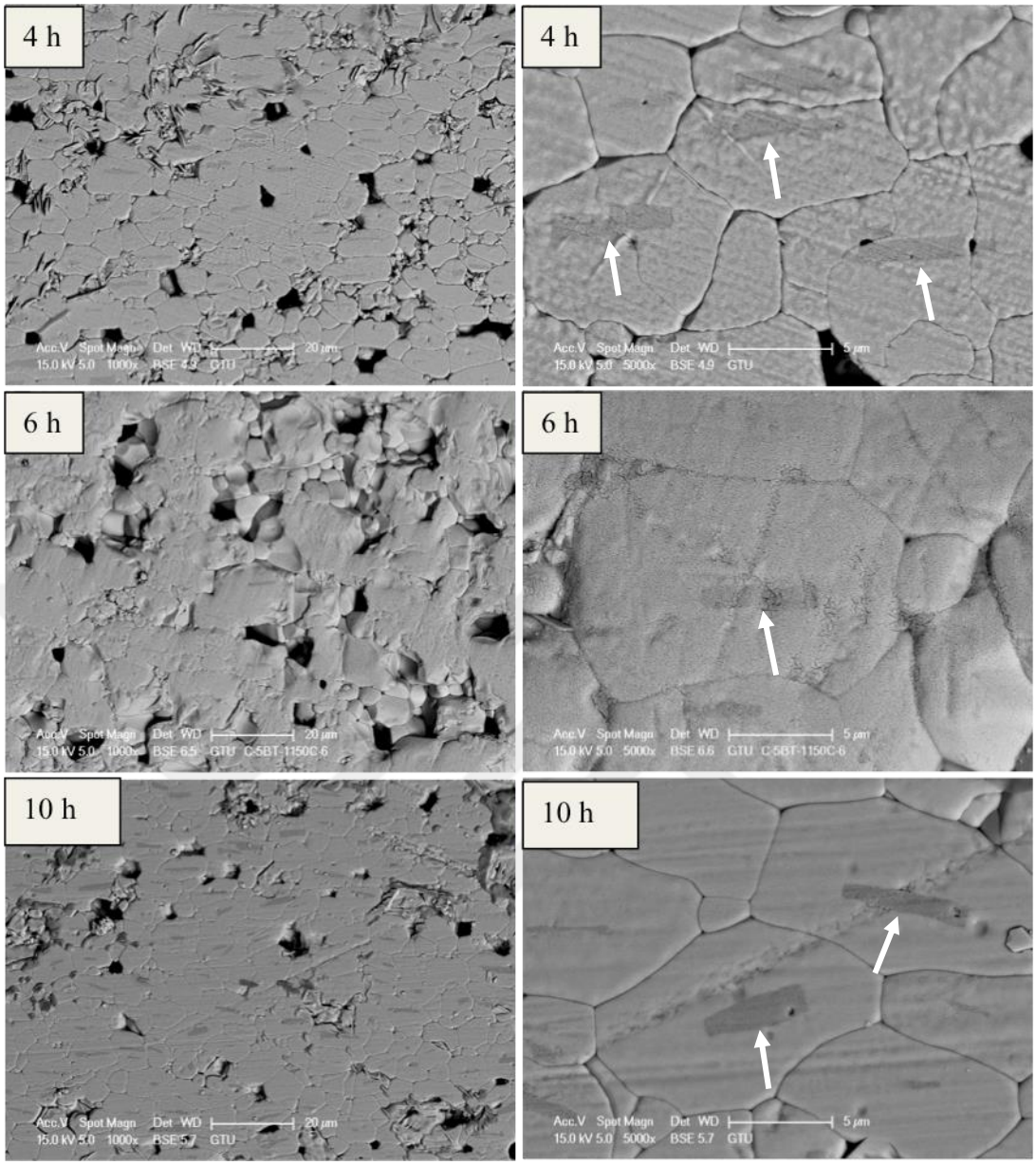

Figure 4.24: The cross-sectional SEM images of textured tape-casted ceramics with 5% BT produced from starting powder II and sintered at different durations.

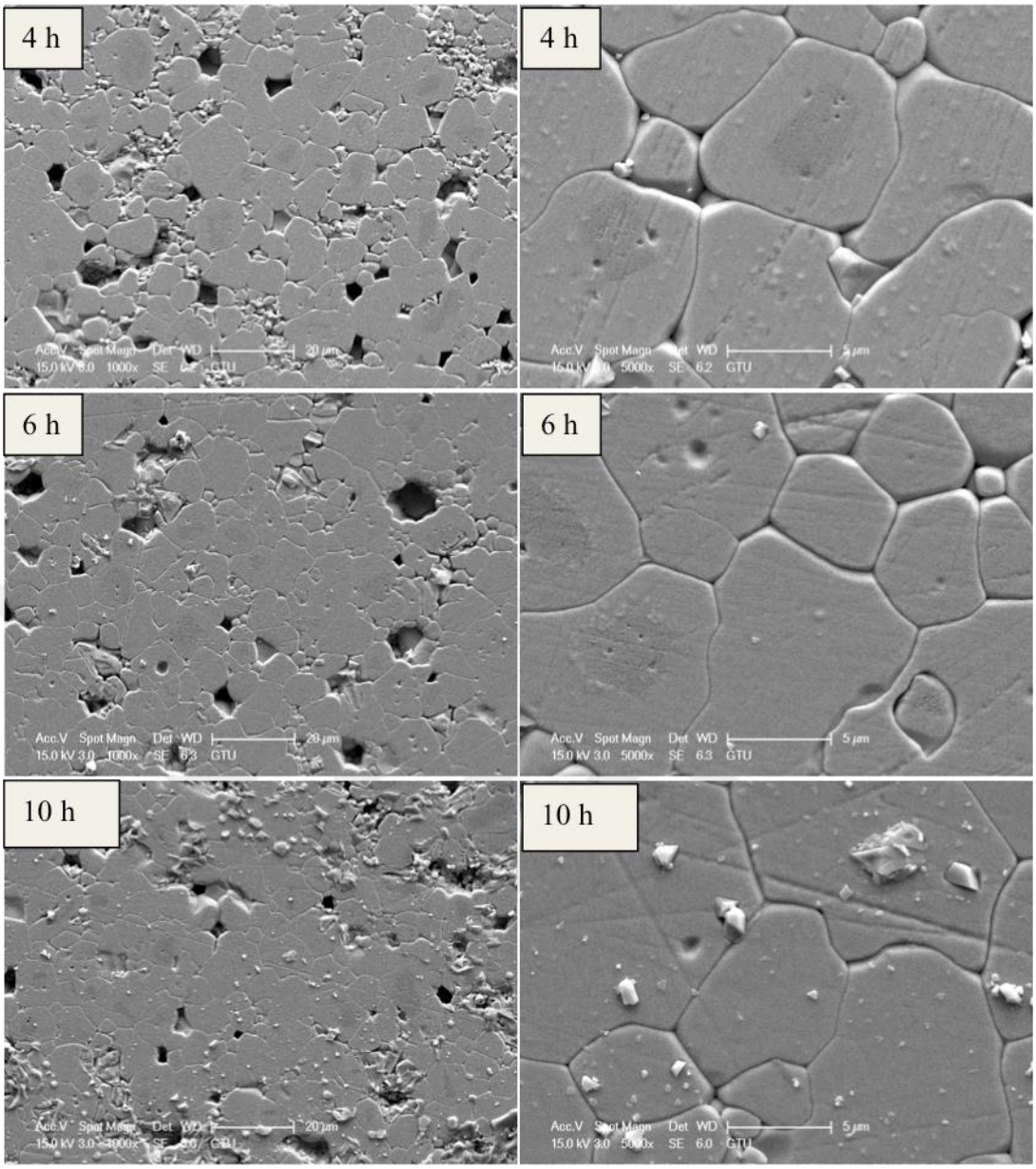

Figure 4.25: The surface SEM images of textured tape-casted ceramics with 5% BT produced from starting powder II and sintered at different durations.

4.5 Electrical Measurements

In this section, polarization versus electric field hysteresis loops (P – E), strain curves, the change of polarization and maximum polarization as a function of temperature and the change of the dielectric constant and dielectric loss as a function of temperature of 0.9PMN-0.1PT ceramics were shown and discussed by the use of graphics and tables. All measurements were performed at 30 kV/cm and 300 – 500 ms periods.

4.5.1 Piezoelectric and Ferroelectric Measurements

As shown in Figure 4.26 and Figure 4.27, dry-pressed ceramics from starting powder I, sintered at 1150°C for 2 h, 4 h, 6 h exhibited relaxor character of ferroelectrics. As seen in Table 4.1, P_{max} and P_r values were similar to each other for all sintering durations. Relaxor ferroelectric materials offered relatively high electric field-induced strain (avareage 0.1 %) with a minimal hysteresis effect [31].

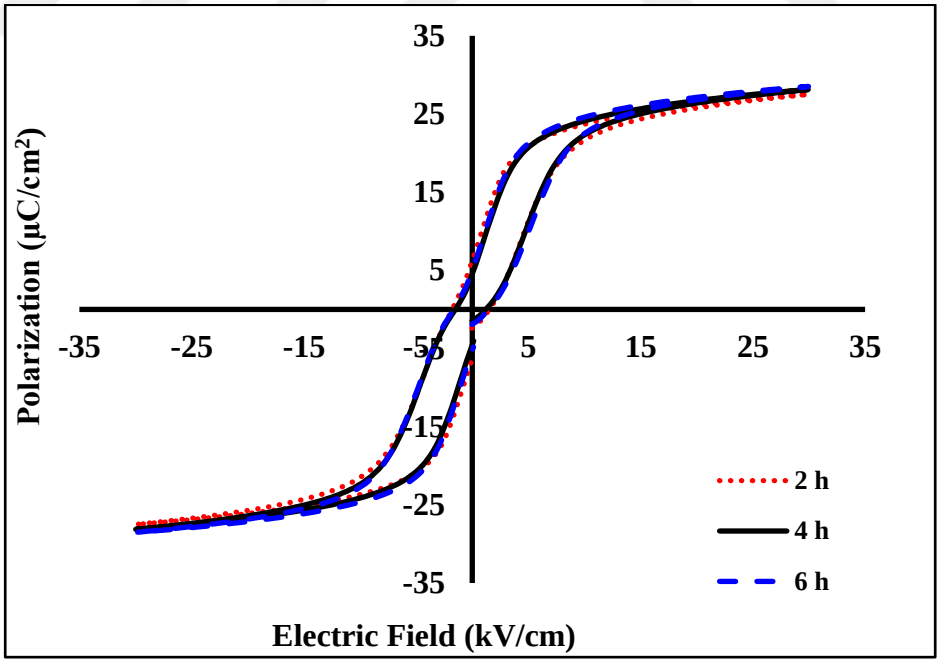

Figure 4.26: The P – E hysteresis loops of dry-pressed ceramics produced from starting powder I and sintered at different durations.

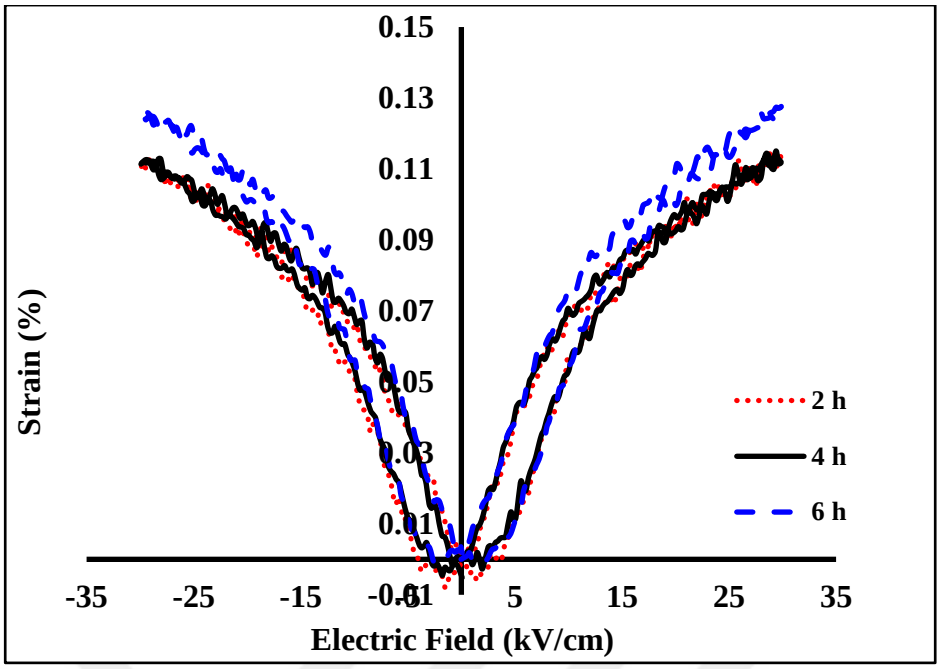

Figure 4.27: The field induced strain curves of dry-pressed ceramics produced from starting powder I and sintered at different durations.

Table 4.1: Electrical properties of dry-pressed ceramics produced from starting powder I and sintered at different durations.

Properties	**Sintering Durations**		
	2 h	**4 h**	**6 h**
P_{max} ($\mu C/cm^2$)	27.49	28.13	28.52
P_r ($\mu C/cm^2$)	6.54	4.81	5.29
E_c (kV/cm)	1.51	1.25	1.48
Max. Strain (%)	0.11	0.11	0.13

As shown in Figure 4.28, dry-pressed ceramics from starting powder II, sintered for different durations exhibited relaxor character of ferroelectrics. Slim hysteresis loops were observed. Figure 4.29 shows typical strain response curves acquired at 0.3 Hz (300 ms). As seen in Table 4.2, P_{max} and P_r values were similar to each other for all sintering durations.

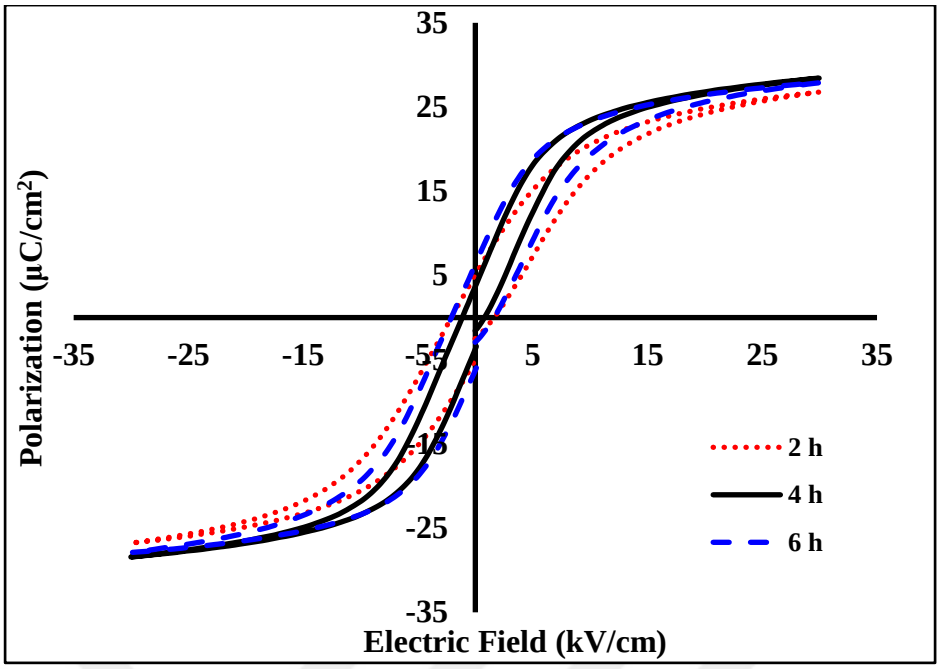

Figure 4.28: The P – E hysteresis loops of dry-pressed ceramics produced from starting powder II and sintered at different durations.

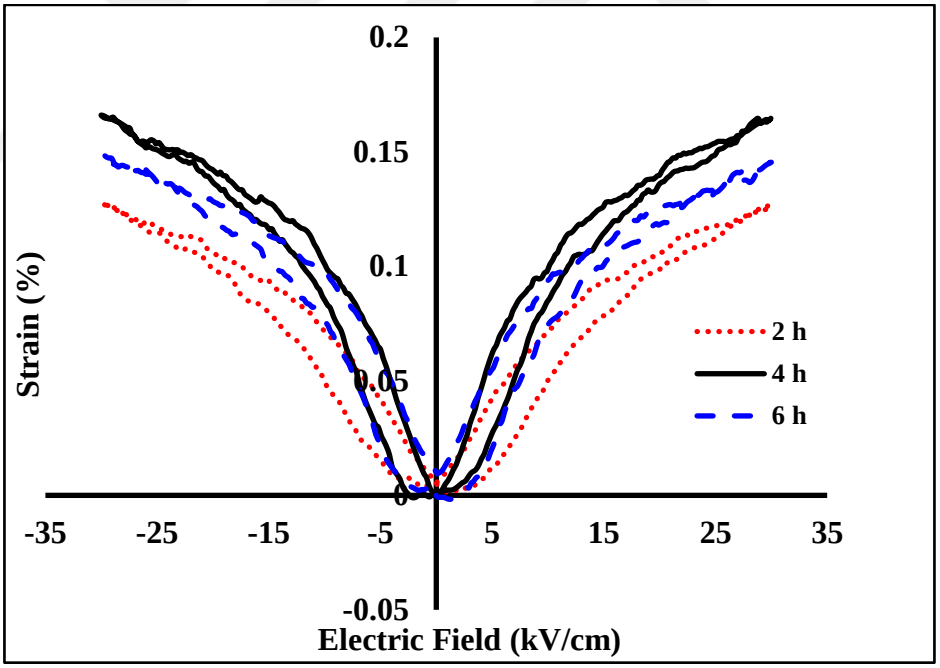

Figure 4.29: The field induced strain curves of dry-pressed ceramics produced from starting powder II and sintered at different durations.

Table 4.2: Electrical properties of dry-pressed ceramics produced from starting powder II and sintered at different durations.

Properties	Sintering Durations		
	2 h	4 h	6 h
P_{max} (μC/cm^2)	26.78	28.43	27.90
P_r (μC/cm^2)	5.05	3.71	6.36
E_c (kV/cm)	1.51	1.25	1.48
Max. Strain (%)	0.12	0.16	0.14

As shown in Figure 4.30 and Figure 4.31, tape-casted ceramics from starting powder I, sintered at 1150°C for 4 h, 6 h, 10 h exhibited relaxor character of ferroelectrics as slim hysteresis loops and electrostrictive strain curves. As seen in Table 4.3, all measurement values were similar to each other for all sintering durations.

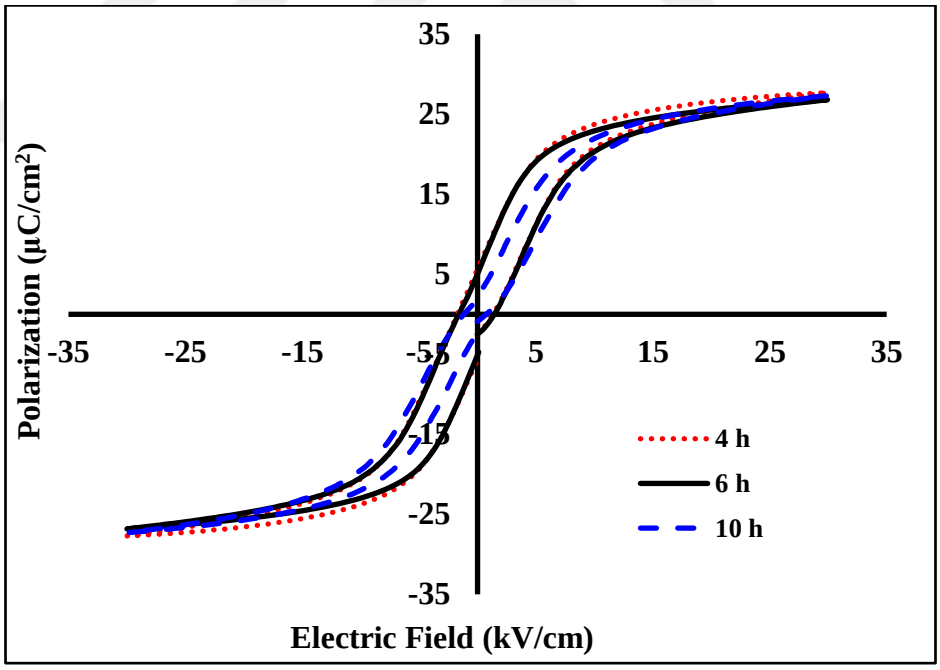

Figure 4.30: The P – E hysteresis loops of random tape-casted ceramics produced from starting powder I and sintered at different durations.

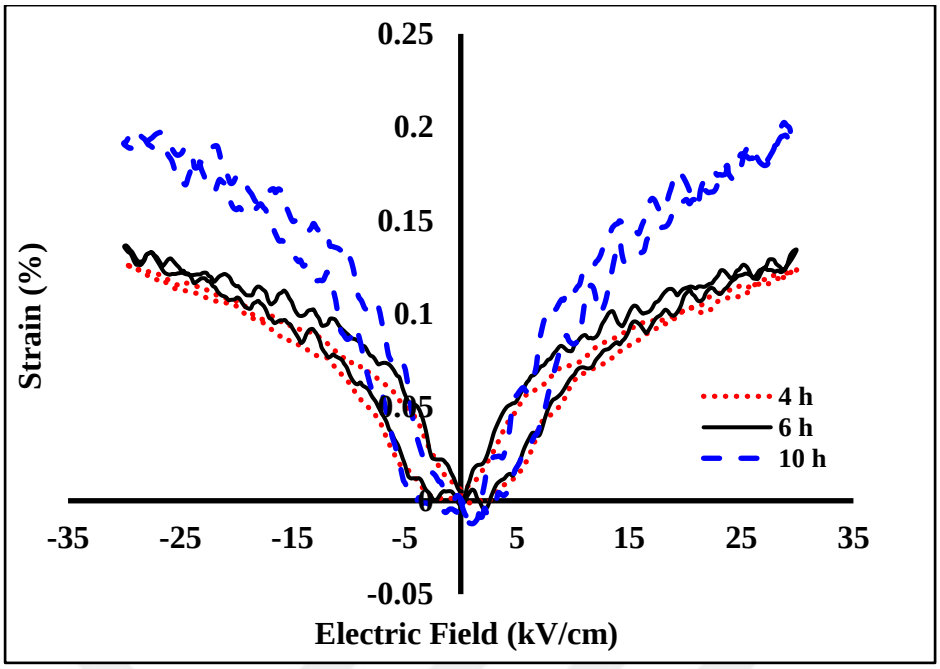

Figure 4.31: The strain curves of random tape-casted ceramics produced from starting powder I and sintered at different durations.

Table 4.3: Electrical properties of random tape-casted ceramics produced from starting powder I and sintered at different durations.

Properties	**Sintering Durations**		
	4 h	**6 h**	**10 h**
P_{max} ($\mu C/cm^2$)	28.09	26.81	27.31
P_r ($\mu C/cm^2$)	4.41	5.06	2.20
E_c (kV/cm)	1.36	1.02	0.98
Max. Strain (%)	0.11	0.13	0.20

As shown in Figure 4.32 and Figure 4.33, tape-casted ceramics from starting powder II, sintered at 1150°C for 4 h, 6 h, 10 h exhibited relaxor character of ferroelectrics as slim hysteresis loops and electrostrictive strain curves. As seen in Table 4.4, all values were similar to each other for all sintering durations.

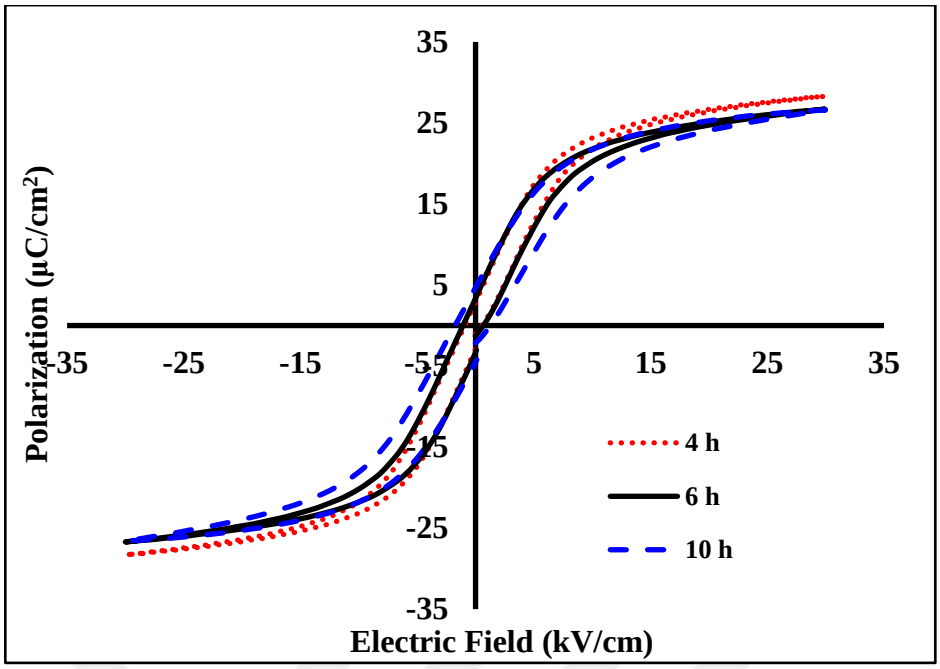

Figure 4.32: The P – E hysteresis loops of tape-casted ceramics produced from starting powder II and sintered at different durations.

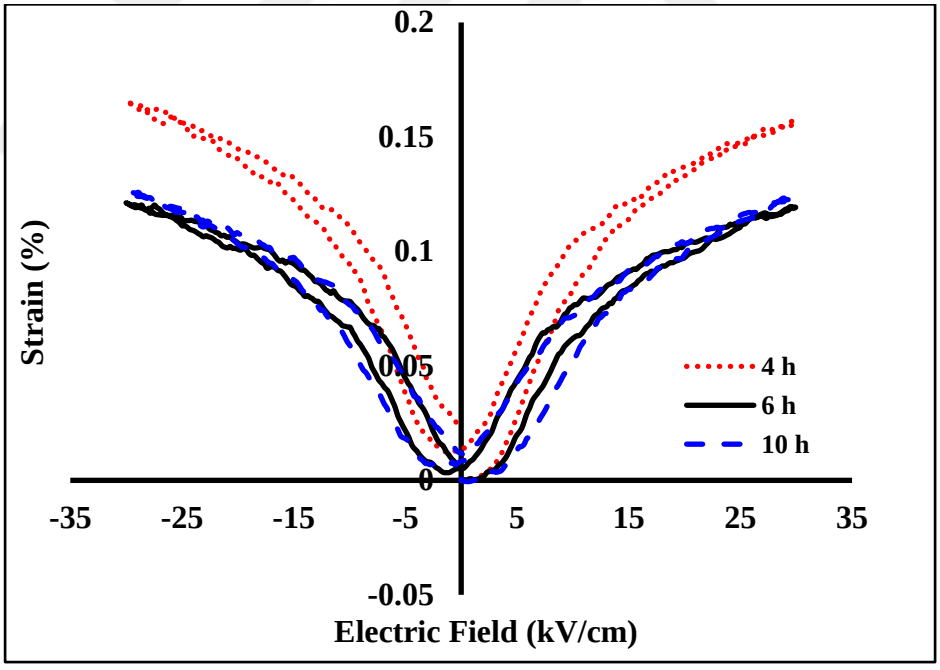

Figure 4.33: The field-induced strain curves of tape-casted ceramics produced from starting powder II and sintered at different durations.

Table 4.4: Electrical properties of random tape-casted ceramics produced from starting powder II and sintered at different durations.

Properties	Sintering Durations		
	4 h	**6 h**	**10 h**
P_{max} ($\mu C/cm^2$)	28.29	26.70	26.60
P_r ($\mu C/cm^2$)	2.89	3.36	5.69
E_c (kV/cm)	1.51	1.25	1.48
Max. Strain (%)	0.12	0.12	0.15

As shown in Figure 4.34 and Figure 4.35, tape-casted ceramics from starting powder I, sintered at 1150°C for 4 h, 6 h, 10 h exhibited relaxor character of ferroelectrics as slim hysteresis loops and electrostrictive strain curves. As seen in Table 4.5, all values were similar to each other for all sintering durations.

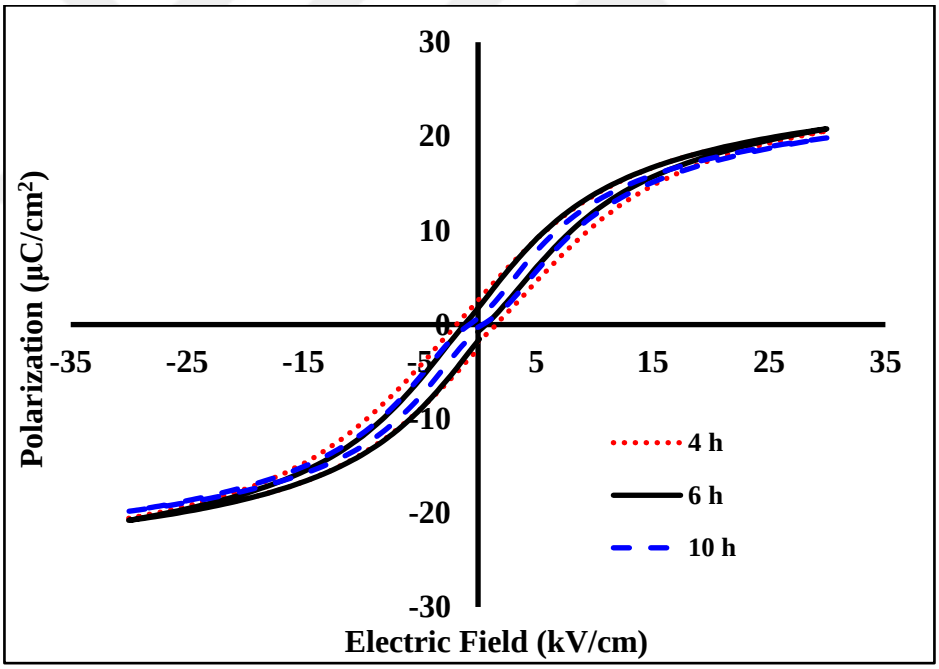

Figure 4.34: The P – E hysteresis loops of textured tape-casted ceramics produced from starting powder I and sintered at different durations.

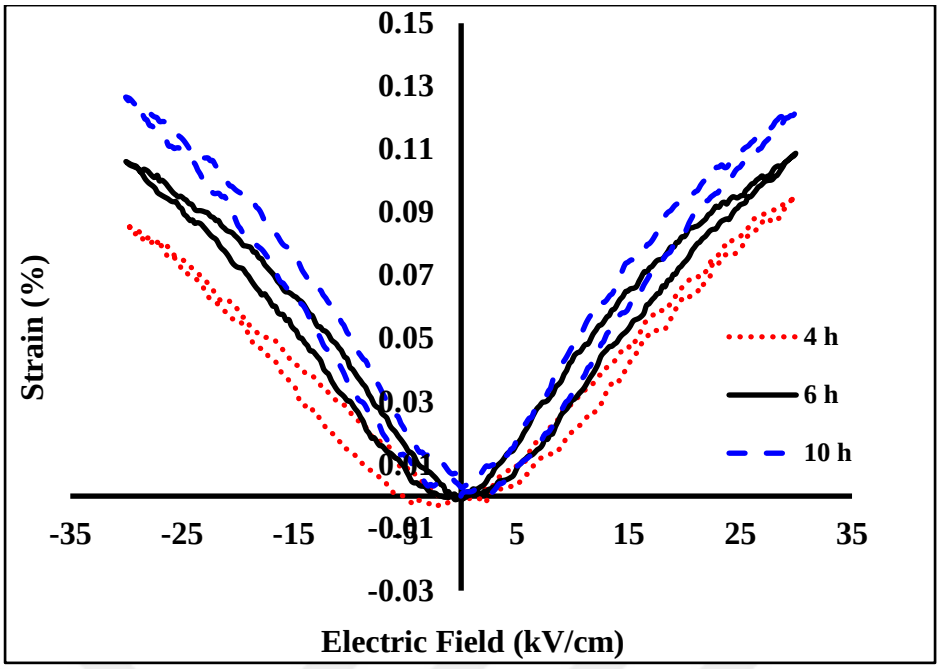

Figure 4.35: The strain curves of textured tape-casted ceramics produced from starting powder I and sintered at different durations.

Table 4.5: Electrical properties of textured tape-casted ceramics produced from starting powder I and sintered at different durations.

	Sintering Durations		
	4 h	**6 h**	**10 h**
P_{max} ($\mu C/cm^2$)	20.58	20.69	19.84
P_r ($\mu C/cm^2$)	2.58	2.25	0.69
E_c (kV/cm)	1.61	0.56	0.34
Max. Strain (%)	0.09	0.11	0.12

As shown in Figure 4.36 and Figure 4.37, tape-casted ceramics from starting powder II, sintered at 1150°C for 4 h, 6 h, 10 h exhibited relaxor character of ferroelectrics as slim hysteresis loops and electrostrictive strain curves. As seen in Table 4.6, all values were similar to each other for all sintering durations.

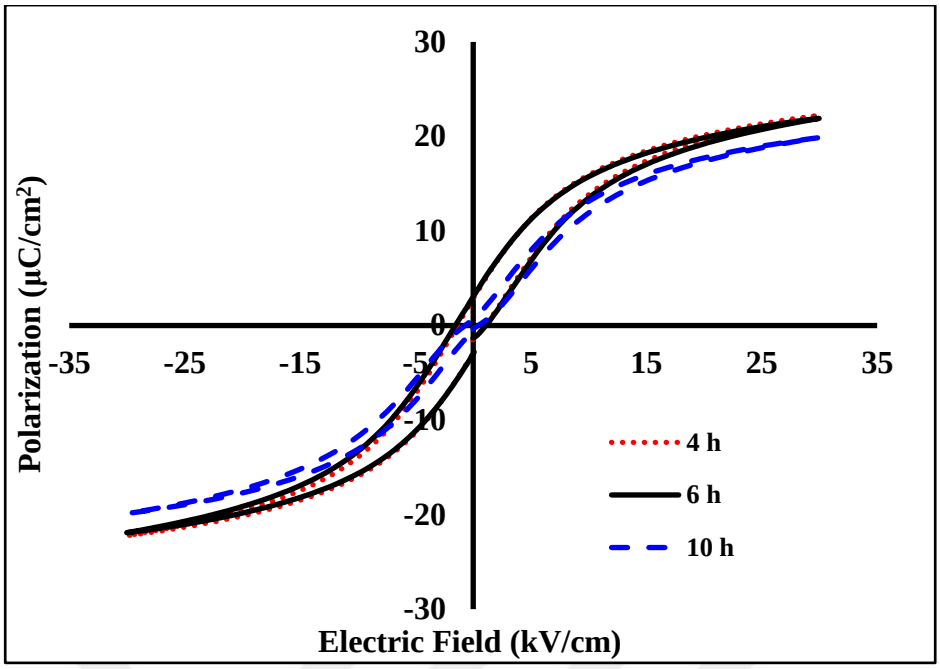

Figure 4.36: The P – E hysteresis loops of textured tape-casted ceramics produced from starting powder II and sintered at different durations.

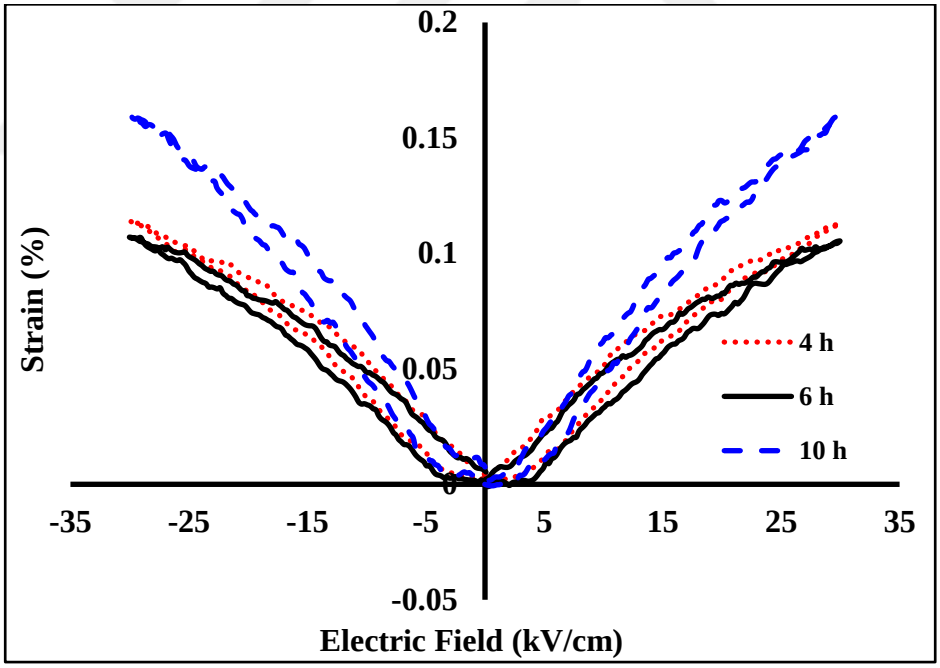

Figure 4.37: The field-induced strain curves of textured tape-casted ceramics produced from starting powder II and sintered at different durations.

Table 4.6: Electrical properties of textured tape-casted ceramics produced from starting powder II and sintered at different durations.

Properties	Sintering Durations		
	4 h	6 h	10 h
P_{max} (μC/cm^2)	22.23	21.85	19.80
P_r (μC/cm^2)	2.84	3.21	0.080
E_c (kV/cm)	0.85	1.11	0.53
Max. Strain (%)	0.16	0.10	0.11

The measured polarization loops at 10, 20, 30, 40, 50, 60, 70, and 80°C and remnant and maximum polarizations as a function of temperature were shown in Figure 4.38 and Figure 4.39. At low temperatures, the remnant polarizations were close to the maximum polarizations for dry-pressed and random tape-casted ceramics. At near the phase transition temperature, where the sharpest transtion of the relaxor, a clear hysteresis loop can also be seen at temperatures higher than the transition region for dry-pressed ceramics. As shown in Figure 4.40, for textured tape-casted ceramics, remnant and maximum polarization values were lower and hysteresis loops were slimmer in comparison to dry-pressed and random tape-casted ceramics. This situation can also be seen from Figure 4.41 clearly.

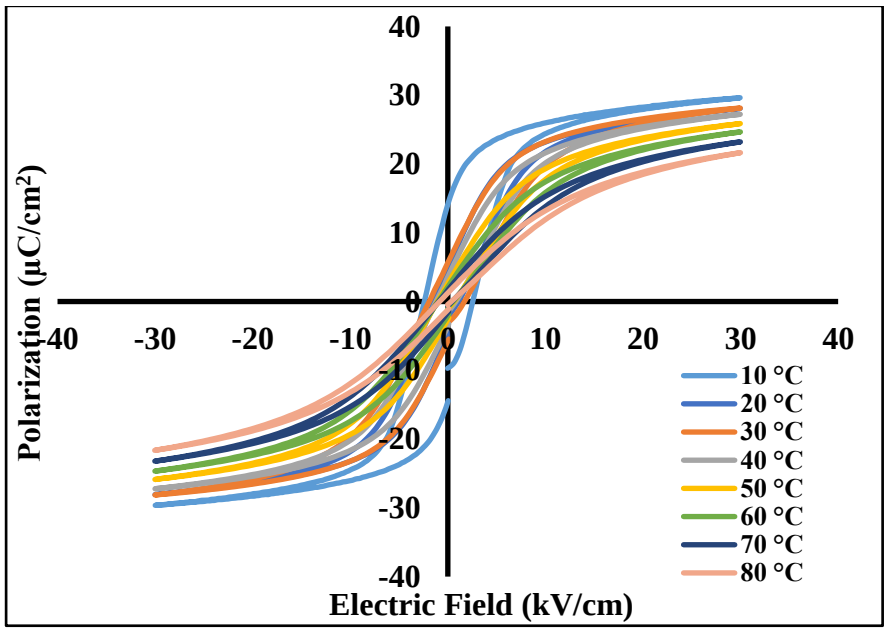

Figure 4.38: The P-E hysteresis loops of dry-pressed sample produced from starting powder I and sintered at 6 h at 30 kV/cm at different temperatures.

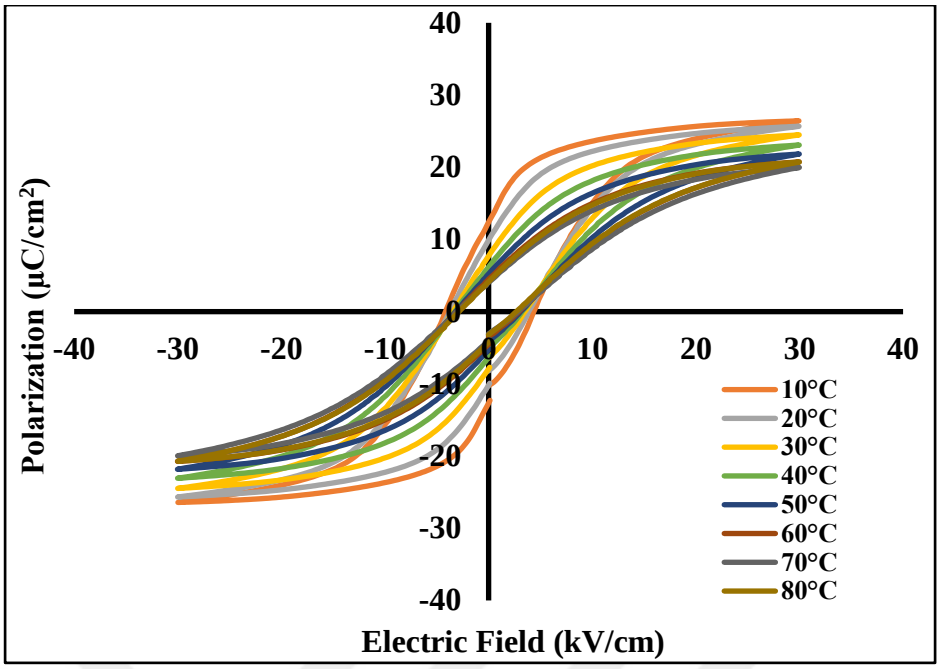

Figure 4.39: The P-E hysteresis loops of random tape-casted sample produced from starting powder I and sintered at 6 h at 30 kV/cm at different temperatures.

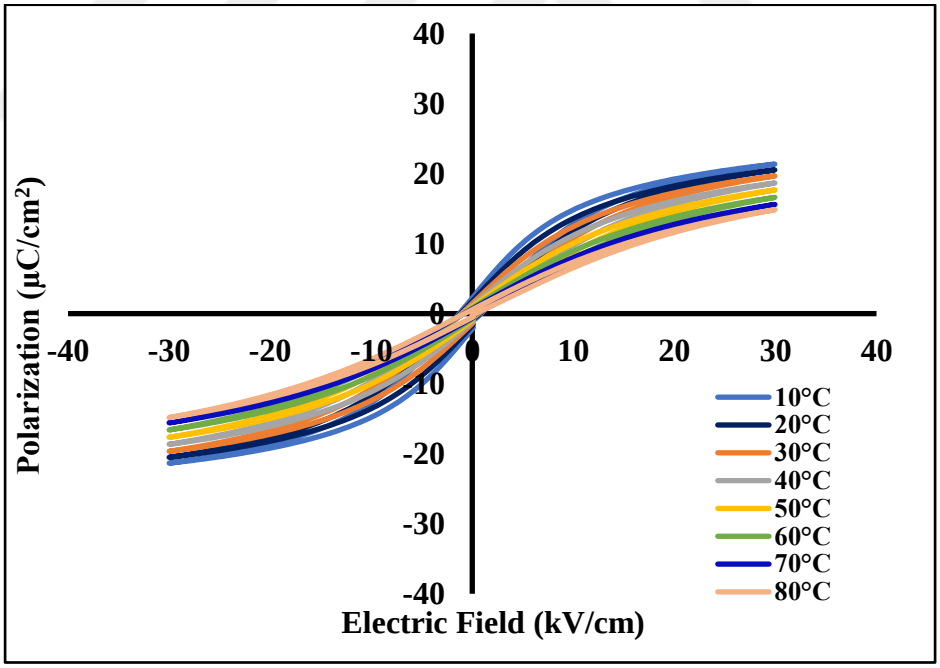

Figure 4.40: The P-E hysteresis loops of textured tape-casted ceramics from starting powder I and sintered at 6 h at 30 kV/cm at different temperatures.

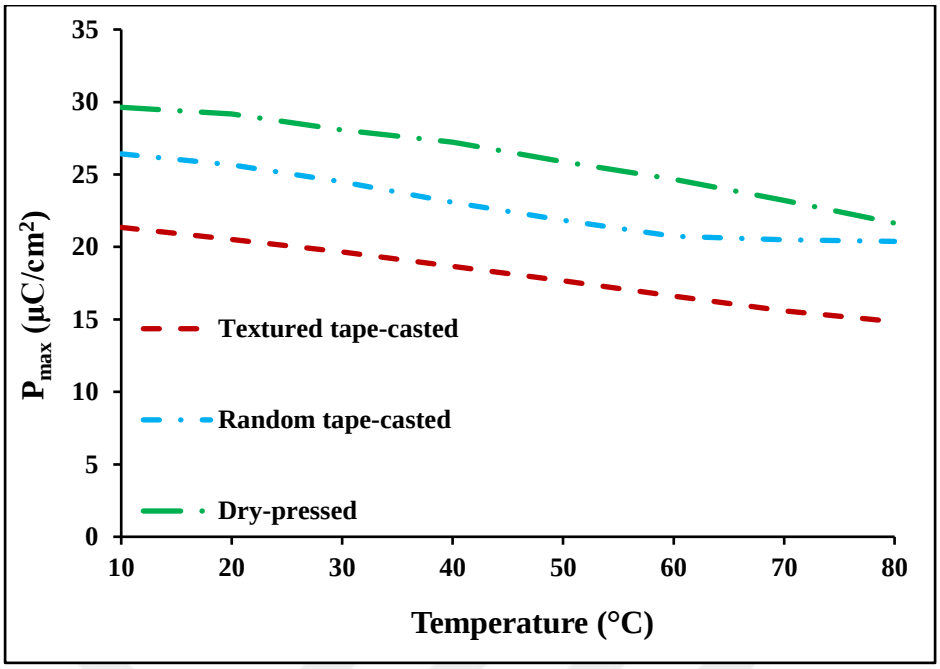

Figure 4.41: The P_{max} change as a function of temperature of dry-pressed and textured tape-casted ceramics from starting powder I and sintered at 6 h at 30 kV/cm.

4.5.2 Dielectric Measurements

The temperature dependence of the dielectric constant and loss was found to be typical for relaxor-type ferroelectrics as shown in Figure 4.42, with strong frequency dispersion at lower temperatures where the Curie temperature (T_c) of the dielectric constant lies [32]. The basic features of the dielectric behavior are the following; There is a broad peak in the dielectric constant as a function of temperature. Curie temperature (T_c) changes with frequency. With increasing frequency, T_c increases, while the magnitude of the peak decreases. There is a strong dielectric dispersion in radio frequency region around and below T_c [33].

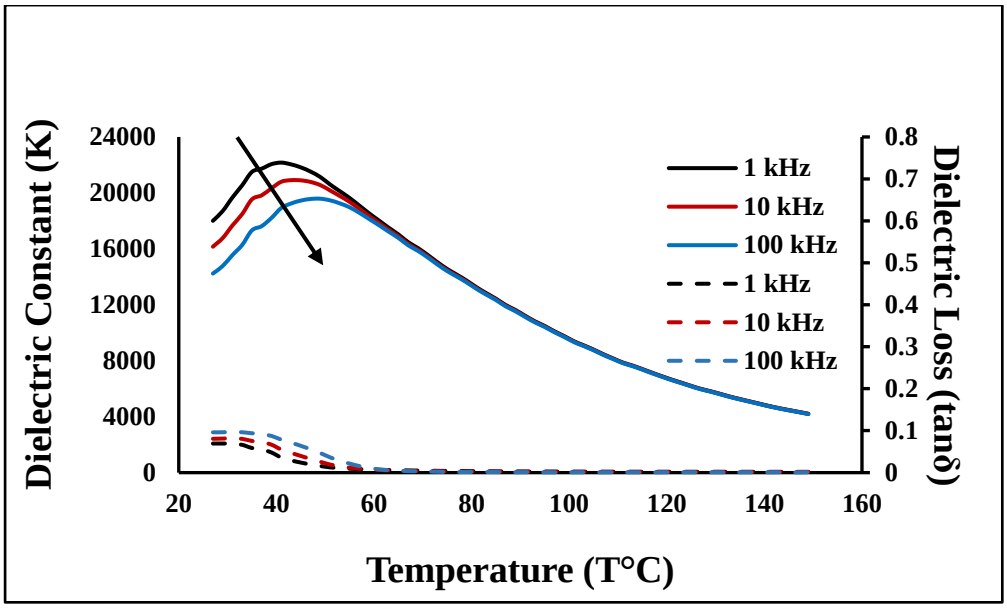

Figure 4.42: The dielectric constant and dielectric loss of dry-pressed ceramic produced from starting powder I and sintered at 6 h at 1, 10, 100 kHz.

The temperature dependence of the dielectric constant (K) and dielectric loss (tanδ) of dry-pressed samples produced from starting powder I at different sintering durations (2 h, 4 h and 6 h) was shown in Figure 4.43. Values of K and tanδ at room temperature were found to be 13347, 15617, 14771 and 0.1, 0.1, 0.09 for 2 h, 4 h, 6 h respectively. K exhibited a broad range around 43°C – 49°C. As seen in Table 4.7, Curie temperature increased with increasing sintering duration.

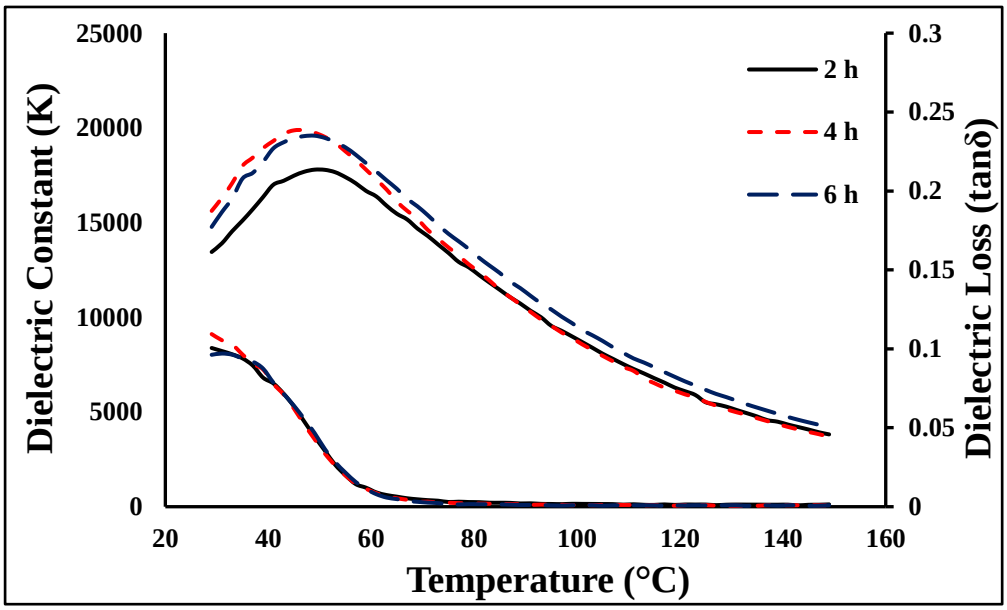

Figure 4.43: The dielectric constant and dielectric loss of dry-pressed ceramics produced from starting powder I and sintered at different durations at 100 kHz.

Table 4.7: Dielectric properties of dry-pressed ceramics produced from starting powder I and sintered at different durations.

Properties	**Sintering Durations**		
	2 h	**4 h**	**6 h**
K, (RT)	13447	15617	14771
tanδ, (RT)	0.1	0.1	0.09
T_c (°C)	43	47	49

The temperature dependence of the dielectric constant (K) and dielectric loss (tanδ) of random tape-casted samples produced from starting powder I at different sintering durations (4 h, 6 h and 10 h) was shown in Figure 4.44. Values of K and tanδ at room temperature were found to be 12149, 13234, 11763 and 0.09, 0.04, 0.02 for 4 h, 6 h, 10 h respectively. K exhibited a broad range around 49°C – 51°C. As seen in Table 4.8, Curie temperature increased with increasing sintering duration.

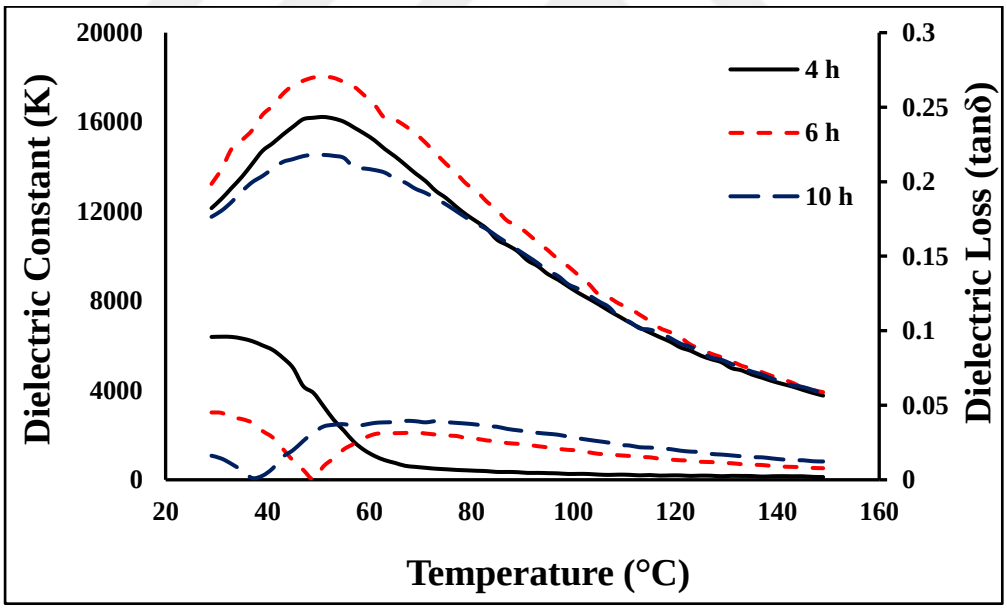

Figure 4.44: The dielectric constant and the dielectric loss of random tape-casted ceramics produced from starting powder I and sintered at different durations at 100 kHz.

Table 4.8: Dielectric properties of random tape-casted ceramics produced from starting powder I and sintered at different durations.

Properties	**Sintering Times**		
	4 h	**6 h**	**10 h**
K, (RT)	12149	13234	11763
tanδ, (RT)	0.09	0.04	0.02
T_c (°C)	51	51	49

The temperature dependence of the dielectric constant (K) and dielectric loss (tanδ) of textured samples produced from starting powder I at different sintering durations (4 h, 6 h and 10 h) was shown in Figure 4.45. Values of K and tanδ at room temperature were found to be 11184, 11653, 9242 and 0.05, 0.13, 0.02 for 4 h, 6 h, 10 h respectively. K exhibited a broad range around 41°C – 49°C. As seen in Table 4.9, Curie temperature increased with increasing sintering duration.

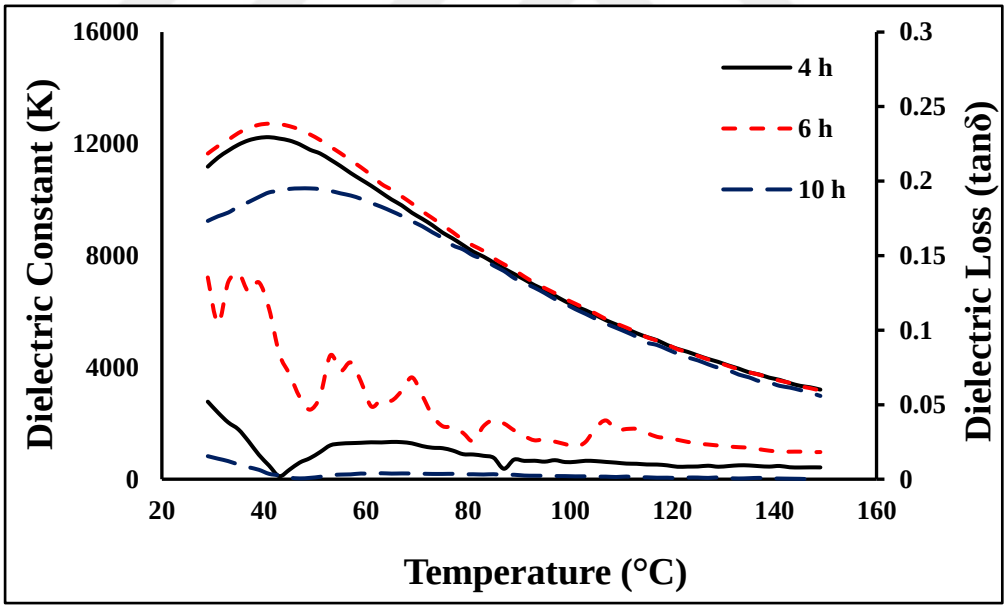

Figure 4.45: The dielectric constant and the dielectric loss of textured tape-casted ceramics with 5% BT produced from starting powder I and sintered at different durations at 100 kHz.

Table 4.9**:** Dielectric properties of textured tape-casted ceramics with 5% BT produced from starting powder I and sintered at different durations.

Properties	**Sintering Times**		
	4 h	**6 h**	**10 h**
K, (RT)	11184	11653	9242
tanδ, (RT)	0.05	0.13	0.02
T_c (°C)	41	41	49

The temperature dependence of the dielectric constant (K) and dielectric loss (tanδ) of dry-pressed samples from starting powder II at different sintering durations (2 h, 4 h and 6 h) was shown in Figure 4.46. Values of K and tanδ at room temperature were found to be 10949, 13276, 13166 and 0.05, 0.1, 0.1 for 2 h, 4 h, 6 h respectively. K exhibited a broad range around 39°C – 49°C. As seen in Table 4.10, Curie temperature increased with increasing sintering duration.

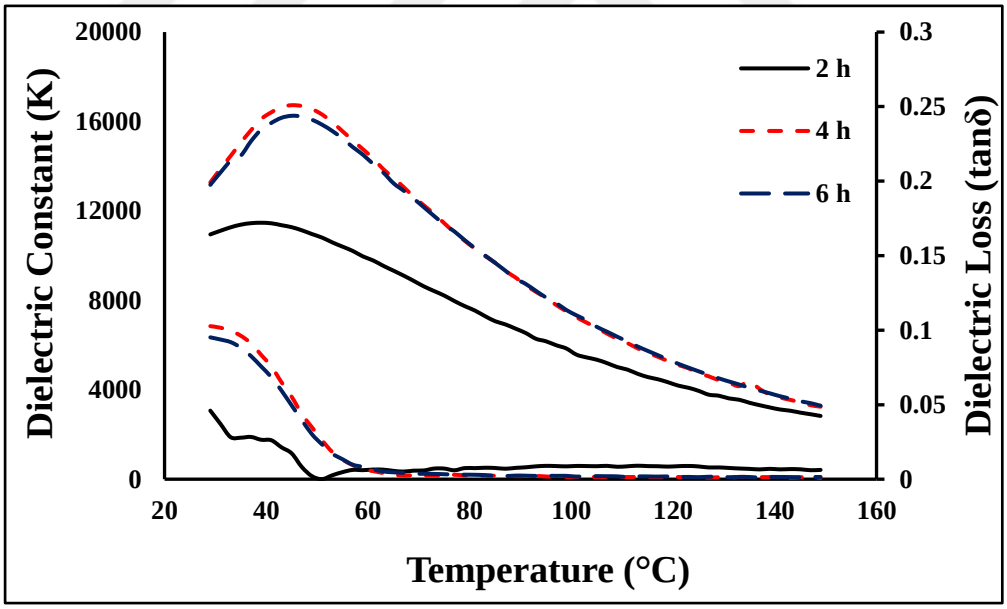

Figure 4.46: The dielectric constant and the dielectric loss of dry- pressed ceramics produced from starting powder II and sintered at different durations at 100 kHz.

Table 4.10: Dielectric properties of dry-pressed ceramics produced from starting powder II and sintered at different durations.

Properties	**Sintering Durations**		
	2 h	**4 h**	**6 h**
K, (RT)	10949	13276	13166
tanδ, (RT)	0.05	0.1	0.1
T_c (°C)	39	45	49

The temperature dependence of the dielectric constant (K) and dielectric loss (tanδ) of random tape-casted samples produced from starting powder II at different sintering durations (4 h, 6 h and 10 h) was shown in Figure 4.47. Values of K and tanδ at room temperature were found to be 19361, 15617, 13384 and 0.09, 0.08, 0.09 for 4 h, 6 h, 10 h respectively. K exhibited a broad range around 45°C – 47°C. As seen in Table 4.11, Curie temperature decreased with increasing sintering duration.

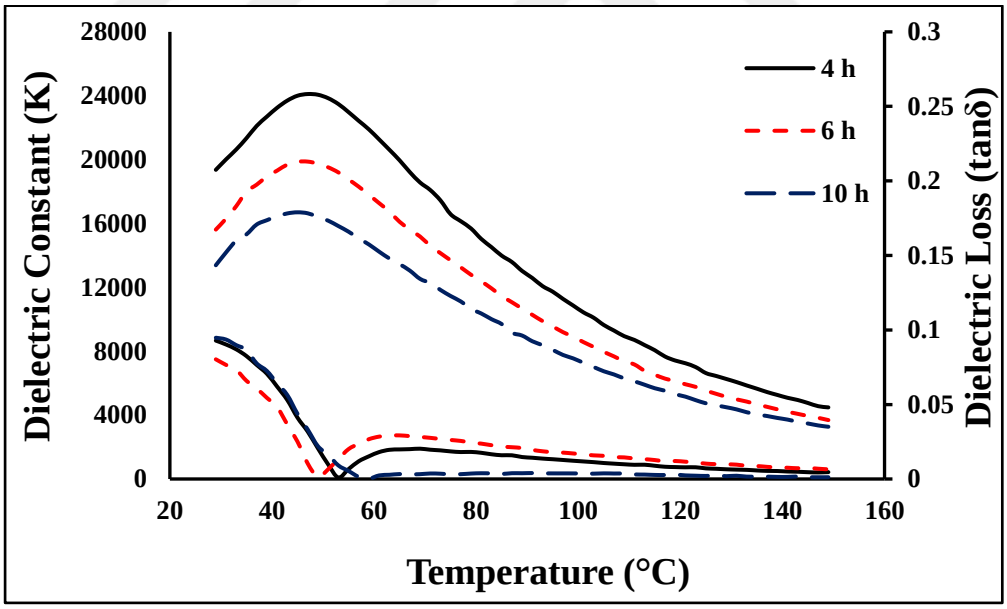

Figure 4.47: The dielectric constant and the dielectric loss of tape-casted ceramics produced from starting powder II and sintered at different durations at 100 kHz.

Table 4.11: Dielectric properties of random tape-casted ceramics produced from starting powder II and sintered at different durations at 100 kHz.

Properties	**Sintering Times**		
	4 h	**6 h**	**10 h**
K, (RT)	19361	15617	13384
tanδ, (RT)	0.09	0.08	0.09
T_c (°C)	47	47	45

The temperature dependence of the dielectric constant (K) and dielectric loss (tanδ) of textured samples produced from starting powder II at different sintering durations (4 h, 6 h and 10 h) was shown in Figure 4.48. Values of K and tanδ at room temperature were found to be 13918, 13114, 12929 and 0.06, 0.09, 0.1 for 4 h, 6 h, 10 h respectively. K exhibited a broad range around 43°C – 45°C. As seen in Table 4.12, Curie temperature increased with increasing sintering duration.

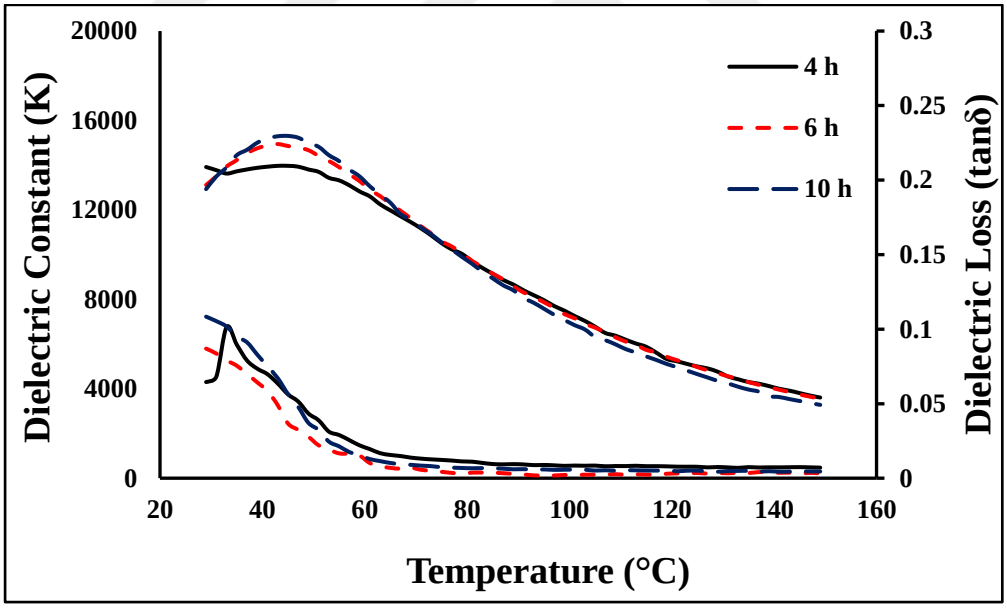

Figure 4.48: The dielectric constant and the dielectric loss of textured tape-casted ceramics with 5% BT produced from starting powder II and sintered at different durations at 100 kHz.

Table 4.12: Dielectric properties of textured tape-casted ceramics with 5% BT produced from starting powder II and sintered at different durations at 100 kHz.

Properties	**Sintering Times**		
	4 h	**6 h**	**10 h**
K, (RT)	13918	13114	12929
tanδ, (RT)	0.06	0.09	0.1
T_c (°C)	43	43	45

5. CONCLUSION

Consequently, in this study; the samples of 0.9PMN-0.1PT were prepared with two methods as dry pressing and tape casting. Moreover, $BaTiO_3$ template particles were synthesized by molten salt synthesis method and were used to texture the compositions with ratio of 5%-vol. 0.9PMN-0.1PT powder I and powder II calcined at 800°C and 850°C for 4 h respectively and these samples were sintered at 1150°C for 2 h, 4 h, 6 h and 10 h. Ceramic samples, sintered at 1150°C, generally crystallize in the perovskite structure without any secondary phases (pyrochlore). As electrical mesaurement results, the values of electrical mesaurement of dry-pressed and random tape-casted samples were similar to each other. All samples exhibited relaxor character of ferroelectrics with slim hysteresis loops and electrostrictive strain curves. The lotgering factor's values of textured tape-casted samples produced from starting powder II were higher than textured tape-casted samples produced from starting powder I. Ferroelectric and dielectric properties of all textured samples were similar to each other. Ferroelectric and dielectric properties of dry-pressed and random tape-casted ceramics were better than textured ceramics.

In future, electrocaloric effect of these samples will be performed in detail.

REFERENCES

[1] Uchino K., (2000), “Ferroelectric Devices”, Marcel Dekker, Inc.

[2] Haertling G. H., (1999), “Ferroelectric ceramics: history and technology”, Journal of the American Ceramic Society, 82 (4), 797-818.

[3] Shrout T. R., Halliyal A., (1987), “Preparation of Lead-Based Ferroelectric Relaxors for Capasitors”, American Ceramic Society Bulletin, 66 (4) 704–11.

[4] Swartz S. L., Shrout T. R., (1982), “Fabrication of Perovskite Lead Magnesium Niobate”, Materials Research Bulletin, 17:10, pp:1245-1250.

[5] Park S. E., Shrout T. R., (1997), “Ultrahigh strain and piezoelectric behavior in relaxor based ferroelectric single crystals”, Journal of Applied Physics, 82 (4), 1804-1811.

[6] Carter C. B., Norton M. G., (2007), “Ceramic Materials: Science and Engineering”, Springer Science & Business Media, Berlin.

[7] Babooram K., Ye Z. G., (2004), "Polyethylene glycol-based new solution route to relaxor ferroelectric $0.65Pb(Mg_{1/3}Nb_{2/3})O_3–0.35PbTiO_3$", Chemistry of materials, 16 (25), 5365-5371.

[8] Newnham R. E., (2005), “Properties of Materials-Anisotropy, Symmetry and Structure”, Oxford University Press.

[9] Kao K. C., (2004), “Dielectric Phenomena in Solids: With Emphasis on Physical Concepts of Electronic Processes”, Boston, MA.

[10] Buchanan R. C., (1991), “Ceramic Materials for Electronics”, Marcel Dekker Inc. New York.

[11] Kalem V., (2011), “Development of Piezoelectric Ceramics for Ultrasonic Motor Applications”, Ortadoğu Teknik Üniversitesi, Ankara.

[12] Goodman G., (1953), “Ferroelectric Properties of Lead Metaniobate”, Journal of the American Ceramic Society, 36 (11), 368- 372.

[13] Barsoum M. W., (2003), “Fundamentals of ceramics”, IOP Publishing Ltd.

[14] Trolier-McKinstry S., (2008), “Crystal Chemistry of Piezoelectric Materials” In: Safari A., Akdoğan E. K., Editors, “Piezoelectric and Acoustic Materials for Transducer Applications”, Springer.

[15] Chen Y. H., Uchino K., Shen M., Viehland D., (2001), “Substituent Effects on the Mechanical Quality Factor of $Pb(Mg_{1/3}Nb_{2/3})O_3$-$PbTiO_3$ and $Pb(Sc_{1/2}Nb_{1/2})O_3$-$PbTiO_3$ ceramics”, Journal of Applied Physics, 90 (3), 1455.

[16] Cross L. E., (1987), “Relaxor Ferroelectrics”, Ferroelectrics, 76, 241–67.

[17] Smolenskii G. A., Agranovuskaya A. I., (1959), “Dielectric Polarization of a Number of Complex Compounds”, Soviets. Physics Solid State, 1, 1429–37.

[18] Moulson A., Herbert J., (2003), “Piezoelectric ceramics”, Electroceramics: Materials, Properties, Applications, 2nd Edition, 339-410.

[19] Shrout T. R., Fielding J. Jr., (1990), “Relaxor Ferroelectric Materials” Proceeding IEEE 1990 Ultrason. Symposium, 711–20.

[20] Bokov V. A., Mylnikova I. E., (1960), “Piezoelectric Properties of New Compound Single Crystals with Perovskit Structure”, Soviet Physics Solid State, 2, 2728–32.

[21] Kimura T., (2006), “Application of texture engineering to piezoelectric ceramics”, Journal of The Ceramic Society of Japan, 114 (1), 15-25.

[22] Chen W., Kinemuchi Y., Tamura T., Watari K., Miwa K., (2006), “Grain-oriented $Bi_4Ti_3O_{12}$ ferroelectric ceramics prepared by magnetic alignment”, Journal of the American Ceramic Society, 89 (2), 490-493.

[23] Messing G. L., Troiler-Mckinstry S., Sabolsky F. M., Duran C., Kwon S., Brahmaroutu B., Park P., Yılmaz H., Rehing P. W., Ecilel K. B., Suvacı E., Seabaugh M., Oh K. S., (2004), “Templated grain growth of textured piezoelectric ceramics”, Critical Reviews in Solid State and Material Sciences, 29:45-96.

[24] Seabaugh M. M., Cheney G. L., Hasinska K., Azad A. M., Sabolsky E. M., Swartz S. L. Dawson W. J., (2004), “Development of a Templated Grain Growth System for Texturing Piezoelectric Ceramics.

[25] Sabolsky E. M., Trolier-McKinstry S., Messing G. L., (2003), “Dielectric and piezoeletric properties of <001> fiber-textured $0.675Pb(Mg_{1/3}Nb_{2/3})O_3–0.325PbTiO_3$ ceramics”, Journal of Applied Physics, 93 (7), 4072-4080.

[26] Lotgering F., (1959), “Topotactical reactions with ferrimagnetic oxides having hexagonal crystal structures-I”, Journal of Inorganic and Nuclear Chemistry, 9 (2), 113-123.

[27] Ananta S., Brydson R., Thomas N. W., (1999), “Synthesis, Formation and Characterisation of $MgNb_2O_6$ Powder in a Columbite-like Phase”, Journal of the European Ceramic Society, 19, 355-362.

[28] Cavalheiro A. A., Zaghete M. A., Paiva Santos C. O, Varela J. A., Longo E., (1999), “Influence of Synthesis and Processing Parameters of the Columbite Precursor on the Amount of Perovskite PMN”, Materials Research. 2, 4.

[29] Menşur-Alkoy E., (2007), "Katkılı ve Katkısız Antiferroelektrik Kurşun Zirkonat İnce Film Sığaçların Elektriksel Özelliklerinin İncelenmesi", Doktora Tezi, Kocaeli Üniversitesi.

[30] Berksoy-Yavuz A., Menşur-Alkoy E., (2018), "Enhanced Soft Character of Crystallographically Textured Mn-Doped Binary 0.675[$Pb(Mg_{1/3}Nb_{2/3})O_3$]–0.325 [$PbTiO_3$] Ceramics", Journal of Electronic Materials, 47 (11), 6557-6566.

[31] Skulski R., Wawrzała P., Ćwikiel K., Bochenek D., (2007), "Dielectric and Electromechanical Behaviors of PMN-PT Ceramic Samples", Journal of Intelligent Material Systems and Structures, 18 (10), 1049-1056.

[32] Hagberg J., Uusimäki A., Jantunen H., (2008), "Electrocaloric characteristics in reactive sintered $0.87Pb(Mg_{1/3}Nb_{2/3})O_3$–$0.13PbTiO_3$", Applied Physics Letters, 92(13), 132909.

[33] Cheng Z. Y., Katiyar R. S., Yao X., Guo A., (1997), "Dielectric behavior of lead magnesium niobate relaxors", Physical Review B, 55(13), 8165.

BIOGRAPHY

Yusuf KILIÇ was born in Fatih, İstanbul in 1989. He finished his high school education in 2006. In the same year, he started to Anadolu University, Physics and Materials Science and Engineering department. He started to Master of Science education in Gebze Technical University, Materials Science and Engineering in 2018.